Chemical Geology 659 (2024) 122152

Contents lists available at ScienceDirect

Chemical Geology

journal homepage: www.elsevier.com/locate/chemgeo

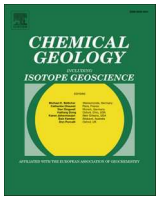

In situ investigation of the atomic structure of carbonate-silicate liquids at high pressure-temperature and spectroscopic characterization of the recovered quenched glasses

Veronica Stopponi [a,b,*], Annalisa D'Arco [c], Yoshio Kono [d], Federica Piccirilli [b], Brent T. Poe [e], Stefano Lupi [c], Manuela Nazzari [f], Lucia Pappalardo [g], Giulia Marras [a], Michele Zacchigna [b], Craig E. Manning [h], Claudia Romano [i], Vincenzo Stagno [a,**]

[a] Department of Earth Sciences, Sapienza University of Rome, Italy
[b] CNR - Istituto Officina dei Materiali (IOM), Trieste, Italy
[c] Department of Physics, Sapienza University of Rome, Italy
[d] Department of Physics and Astronomy, Kwansei Gakuin University, Sanda, Japan
[e] Department of Engineering and Geology, University of Chieti-Pescara, Italy
[f] National Institute of Geophysics and Volcanology, Rome, Italy
[g] National Institute of Geophysics and Volcanology, Osservatorio Vesuviano, Italy
[h] Department of Earth, Planetary and Space Sciences, University of California, Los Angeles, CA, USA
[i] Department of Sciences, University of Studies Roma Tre, Rome, Italy

ARTICLE INFO

Editor: Don Porcelli

Keywords:
Carbonate-silicate melts
Atomic structure
CO_2 speciation
Vibrational properties of glasses
Metal carbonyls

ABSTRACT

Carbonate-silicate melts that originate in Earth's interior are described as transitional melts which possess compositions intermediate between carbonatitic and basaltic end members. The covariation of key oxides between carbonatite and basalt (e.g., 10–35 wt% SiO_2 and 40–10 wt% CO_2, respectively) is expected to have a strong effect on liquid properties. However, due to their paucity both in the record of terrestrial rocks and as quenched glasses, their molecular structure has remained poorly explored to date. We investigated the atomic structure of a synthetic carbonate-silicate liquid with chemical composition within the CaO-MgO-Al_2O_3-SiO_2-FeO-Na_2O-ClO^--CO_2 oxide system having 18.28 wt% SiO_2 and 22.54 wt% CO_2 using multi-angle energy dispersive X-ray diffraction at pressures (P) and temperatures (T) of 1.4 GPa/1815 °C, 2.6 GPa/1865 °C, 4.3 GPa/1990 °C, 4.4 GPa/1950 °C. The results show that the intermediate range ordering of the structure decreases with an increase of both P and T. Based on this study, the carbonate-silicate magmas at upper mantle P-T conditions are expected to increase their viscosities during their ascent through the mantle as a result of increasing intermediate range ordering upon cooling and decompression. Additionally, spectroscopic measurements were carried out on the quenched glasses at ambient pressure using micro-Raman as well as micro-FTIR in reflection and transmission modes in the mid infrared range. High pressure investigation using micro-FTIR was also conducted. The distribution of Q_n species obtained by deconvolution of the Raman spectra within the aluminosilicate region confirms the depolymerized nature of the quenched glasses as inferred by the low viscosities of the corresponding liquids; peculiar characteristics of the C vibrations would suggest a distorted environment surrounding the network modifying CO_3^{2-} anion. No evidence of molecular CO_2 was detected. Notably, we find evidence of both dissolved molecular CO and CO linked to a metal cation forming carbonyl complexes in the quenched glasses at P-T-fo_2 conditions compatible with a hot Archean upper mantle. This suggests a role for carbonate-silicate magmas as carriers of reduced gaseous C-O-H species towards the early atmosphere along with the mobilization of PGE-elements.

* Corresponding author at: CNR - Istituto Officina dei Materiali (IOM), Trieste, Italy
** Corresponding author.
E-mail addresses: stopponi@iom.cnr.it (V. Stopponi), vincenzo.stagno@uniroma1.it (V. Stagno).

https://doi.org/10.1016/j.chemgeo.2024.122152
Received 24 November 2023; Received in revised form 24 April 2024; Accepted 8 May 2024
Available online 10 May 2024

1. Introduction

Natural magmas are the most efficient carriers of CO_2 from the interior of Earth to the surface and, eventually, out to the atmosphere. Extensive experimental studies were carried out in the last decades to determine phase equilibria and melting conditions at high pressure (P) and temperature (T) of mantle rocks (i.e. peridotites and eclogites) in the presence of oxidized carbon (C^{4+}) (Wyllie and Huang, 1976; Eggler, 1978; Wallace and Green, 1988; Dalton and Wood, 1993; Dalton and Presnall, 1998; Moore and Wood, 1998; Hammouda, 2003; Yaxley and Brey, 2004; Gudfinnsson and Presnall, 2005; Dasgupta and Hirschmann, 2006, 2007; Ghosh et al., 2009, 2014; Litasov and Ohtani, 2009a, 2009b, 2010; Keshav and Gudfinnsson, 2010; Kiseeva et al., 2012, 2013; Green, 2015). These studies show that melts generated at near-solidus conditions are carbonatitic in composition (5–10 wt% SiO_2–40 wt% CO_2) and, by increasing T, progressively dissolve more SiO_2 (10–30 wt %) at the expense of CO_2 (decreasing to ~15 wt%), while the melt fractions modelled on the basis of carbon available in the mantle (Dasgupta et al., 2013; Aiuppa et al., 2021) range from 0.01 wt% to ~1 wt% with transitional melts being stable over relatively large P-T conditions as a function of volatile components (i.e., CO_2 and H_2O). As a result of the combined effect of P, T and bulk rock chemistry, a wide range of melt compositions exists spanning from carbonatite to kimberlite to basalt (Hammouda and Keshav, 2015). The rheological properties of melts in this compositional range likely vary significantly with changing concentrations of network forming vs. modifying cations and the mechanism of CO_2 incorporation in the liquid structure (i.e., dissolved CO_3^{2-} and molecular CO_2). Recently, the viscosity of melts intermediate between carbonate and silicate end members (here termed "transitional") was shown to be about one order of magnitude higher than dolomitic melts at mantle P-T conditions, providing the first experimental evidence of the effect of increasing the amount of tetrahedrally-coordinated Si in ultrabasic magmas on viscosity, mobility and migration rate (Stagno et al., 2020a). Recent implementations that allow experimental measurements of the liquid structure to be performed by X-ray diffraction technique at HP-T (Kono et al., 2014a) provide the opportunity to link changes in viscosity to atomic-scale changes and distortion of the cation-coordinated polyhedra. However, to date, melt structure measurements conducted at high P-T applicable to natural magmatic systems are available only for dolomitic and calcitic liquids representative of carbonatitic melts (Kono et al., 2014b; Hudspeth et al., 2018), melilititic liquids (Stagno et al., 2020b) and liquids representative of basalts erupted at mid-ocean ridges (Sakamaki et al., 2013). No measurements have been conducted in situ on transitional liquids, although their presence at mantle conditions has been established through geochemical (Tappe et al., 2017) and experimental evidence (see Fig. 1 and references in Stagno et al., 2020a).

The P-T dependence of CO_2 incorporation in the melt structure has been mostly investigated through the analyses of the quenched glasses providing, therefore, a valuable information on the solubility of CO_2 for a specific composition. This can be summarized with a gradual increase of CO_2 being dissolved as the melt is less polymerized (see Fig. 2 in Brooker et al., 2011). The effect of P on the CO_2 solubility appears to be gradual for all compositions except in the case of carbonatitic and kimberlitic glasses. While carbonatitic glasses show no P dependence implying that carbonatite rocks at the surface might retain the CO_2 content from the mantle source, kimberlitic melts release most of the dissolved CO_2 below 0.5 GPa, as experimentally observed (Brooker et al., 2011). Importantly, recent data on CO_2 solubility in basaltic and andesitic melts showed that the increase of CO_2 with increasing P is more pronounced than what would be expected from Henry's law (Amalberti et al., 2021), in agreement with molecular dynamics simulations (Guillot and Sator, 2011). In contrast, a negative correlation was established between T and CO_2 solubility in glasses regardless of their composition, with the exception of nephelinitic glasses which instead follow a positive trend (Blank and Brooker, 1994; Brooker et al., 1999). In addition, CO_2 solubility in glasses with a relatively low SiO_2 content varying from ~30 to 45 wt% was observed to increase for decreasing MgO/(MgO + CaO) content (Brooker et al., 2001a; Morizet et al., 2017a).

In contrast, the experimental investigation of the CO_2 solubility in transitional melts has been quite problematic due to the difficulty in quenching these liquids as glasses. Instead, solubilities have been extrapolated from partially crystallized experiments (Brey and Ryabchikov, 1994; Brooker et al., 2011) and atomistic simulations (Guillot and Sator, 2011; Vuilleumier et al., 2015). Moussallam et al. (2015) published data on CO_2 solubility as a function of the P and T of glass synthesis for compositions varying between 18 and 25 wt% SiO_2. Interestingly, a sudden decrease of CO_2 solubility was observed at about 0.1 GPa that would imply a dramatic release of about 10 wt% CO_2 upon decompression. The knowledge of the rheological properties of carbonate-silicate melts and their role as carriers of deep C requires the determination of the CO_2 speciation in these liquids in response to the introduction and increase of tetrahedrally coordinated Si^{4+} cations in the evolving melt structure.

Pioneering experimental studies performed on quenched glasses at room/high P and T using both Fourier-transform infrared (FTIR) and Raman spectroscopy showed that C can dissolve in silicate liquids either as CO_2 molecules or carbonate groups CO_3^{2-} (Brey and Green, 1976; Mysen et al., 1975). Further studies have investigated the effect of P, T and glass composition on the speciation of C within a wide spectrum of natural and synthetic glass compositions (Blank and Brooker, 1994; Mysen and Richet, 2019; Ni and Keppler, 2013). Currently available data suggest that CO_2 dissolves predominantly as carbonate in (ultra) basic glasses (e.g. nephelinites), but as molecular CO_2 in more acidic glasses (e.g. rhyolites, Blank and Brooker, 1994), with the fraction of molecular CO_2 expressed as $CO_2/(CO_2 + CO_3^{2-})$ that increases from 0.1 to 0.9 for SiO_2 contents ranging from 65 to 85 wt%, at least at low T (Brooker et al., 1999; King and Holloway, 2002; Guillot and Sator, 2011; Konschak and Keppler, 2014).

In situ spectroscopic measurements on synthetic CO_2-bearing glasses at HP-T are very rare and only limited to dacite, phonolite, basaltic andesite, and alkali silicate melt at P of 1 atm-11.4 GPa at ambient T to 1000 °C (Konschak and Keppler, 2014).

These experiments are unique in showing that 1) as P increases the dissolved molecular CO_2 is converted into carbonate anion with no distinction between dacitic and phonolitic glasses; 2) alkali silicate and basaltic andesite glasses show no evidence of molecular CO_2 even when heated, contrary to that which is observed for phonolitic and dacitic glasses. Following these results, exsolution of molecular CO_2 from the magma upon decompression is expected to be triggered by free (i.e., not-network forming) carbonate in the case of less polymerized magmas. A similar behavior is expected in the case of more basic-to-ultrabasic compositions such as carbonate-silicate magmas.

Transmission FTIR and Raman spectra of CO_2-rich silicate glasses by Moussallam et al. (2016) showed evidence of the occurrence of dissolved CO_2 only in the form of carbonate instead of molecular CO_2. These glasses, however, are unrepresentative of realistic carbonate-silicate glasses because they are more Ca-rich and Mg-poor than partial melts of carbonated mantle peridotites and eclogites (Fig. 1). Fig. 1 illustrates that glasses investigated by Moussallam et al. (2015, 2016) fall into the field of carbonatites, while compositions explored in this study fall into the wide field of transitional melts in between carbonatites and kimberlites.

The different chemical composition of the transitional melts might result in different spectroscopic properties and CO_2 speciation. Here, we present results relative to the atomic structure of carbonate-silicate transitional melts investigated by multi-angle energy-dispersive X-ray diffraction at HP-T and the characterization of the recovered quenched glasses by micro-Raman spectroscopy at ambient P and micro-FTIR spectroscopy both at ambient and high P. Diffraction data collected on the melt were, then, interpreted in light of recent viscosity

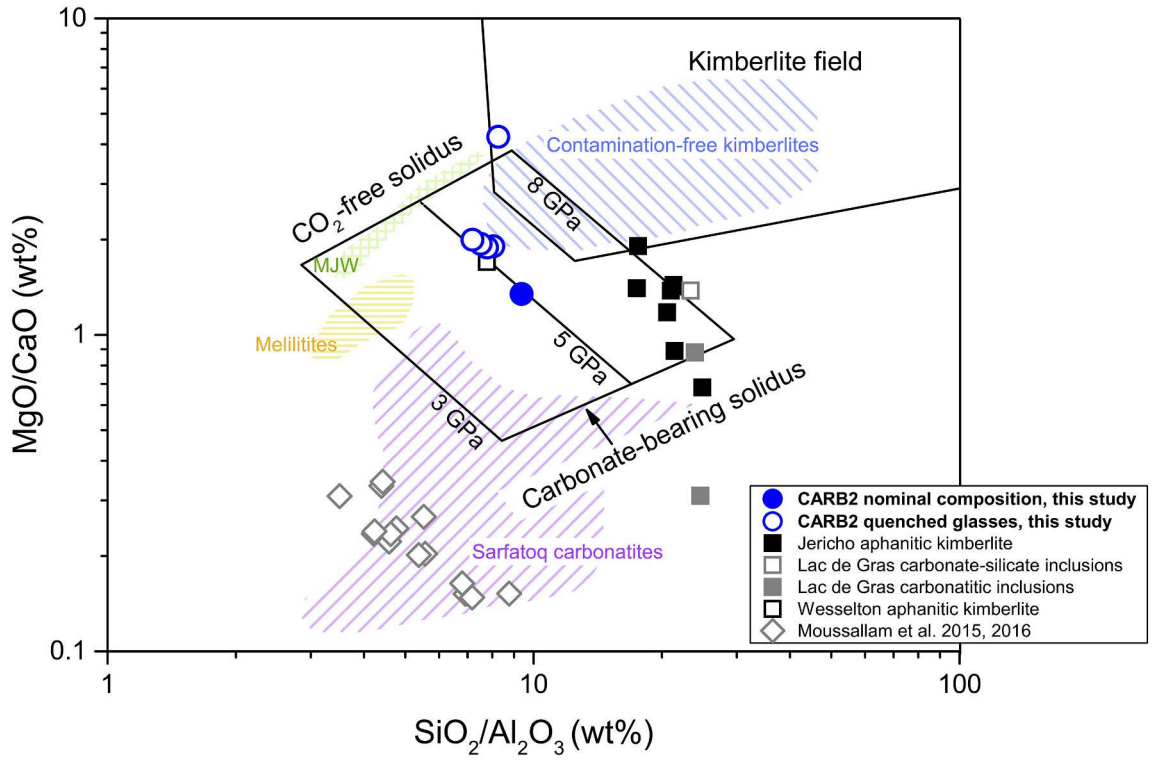

Fig. 1. SiO_2/Al_2O_3 versus MgO/CaO discrimination diagram (Rock, 1991) modified after Gudfinnsson and Presnall (2005) showing both CARB2 starting material and the recovered synthetic glasses from the HP-T experiments in this study compared with natural CO_2-rich volcanic rocks (kimberlite field: Mitchell, 1986; melilitite field: Mitchell, 1996; Jericho: Price et al., 2000, Wesselton: Shee, 1986; Lac de Gras carbonatitic inclusions: Van Achterbergh et al., 2002; Lac de Gras silico-carbonate: Van Achterbergh et al., 2004) along with glasses investigated by Moussallam et al. (2015, 2016). The field MJW stands for the compositions of melts generated in equilibrium with the garnet lherzolite phase assemblage at 3–7 GPa in experiments by Walter (1998).

measurements for these compositions, while spectra from Raman and FTIR analyses were compared with data from literature to establish how the HP-T of synthesis can affect the CO_2 solubility, carbon speciation and silicate network polymerization.

2. Experimental methods and analytical techniques

2.1. Synthetic starting material

The starting sample used in this study is a partially crystallized glass prepared by melting a mixture of oxides and carbonates at ~0.3 GPa and 1410 (±10) °C for 1 h using a non-end loaded piston cylinder (details are in Stagno et al., 2020a). The starting material (CARB2) has the following composition: 18.28 wt% SiO_2, 20.43 wt% CaO, 27.50 wt% MgO, 6.72 wt % FeO, 1.95 wt% Al_2O_3, 1.37 wt% Na_2O, 1.21 wt% ClO^-, and 22.54 wt % CO_2. This chemical composition is representative of the quenched carbonate-silicate melts reported from several experimental studies (Dalton and Presnall, 1998; Moore and Wood, 1998; Gudfinnsson and Presnall, 2005; Brey et al., 2008; Foley et al., 2009; Litasov and Ohtani, 2009a, 2009b; Litasov and Ohtani, 2010; Stagno and Frost, 2010; Brey et al., 2011; Brooker and Kjarsgaard, 2011; Rohrbach and Schmidt, 2011; Kiseeva et al., 2012, 2013; Ghosh et al., 2014; Keshav and Gudfinnsson, 2014). The starting material CARB2 was used for the viscosity measurements reported in Stagno et al. (2020a), followed by the melt structure measurements described here.

2.2. In situ liquid structure measurements

Measurements of the liquid structure were performed at high P-T by in situ multi-angle energy dispersive synchrotron X-ray diffraction (EDXD) technique using the Paris-Edinburgh press at beamline 16BM-B of the Advanced Photon Source at Argonne National Laboratory (Lemont, IL, USA; Kono et al., 2014a). The experimental P was determined using the equation of state of MgO collected from the MgO sleeve (Kono et al., 2010), while the T was raised following the power vs. temperature calibration (Kono et al., 2014a). For each run, the starting material was placed into a graphite capsule and enclosed in the cell assembly described by Stagno et al. (2020a). In some runs an additional layer of $CaCO_3$ about 100 μm thick (run CARB2_1_2016) or San Carlos olivine + Li_2CO_3 of about 100 μm thick (run CARB2_2_2018) was placed in the top-most part of the capsule in order to conduct two viscosity measurements at two different temperatures (i.e. the melting T of CARB2 starting material and melting T of either carbonates or olivine at given pressure) within the same experimental run (Stagno et al., 2020a). Liquid structure measurements were performed just after the viscosity experiments (Stagno et al., 2020a). Series of EDXD patterns were acquired within 3–4 h. The diffraction patterns were collected at fixed 2θ angles of 3° (625 s), 4° (550 s), 5° (500 s), 7° (700 s), 9° (500 s), 12° (500 s), 16° (500 s), 22° (625 s), 28° (1250 s) with a Ge-solid state detector mounted on a 2θ arm on a Huber rotation stage. The X-ray beam was adjusted to the center of the sample using the Prosilica GC1380 high-resolution camera with pixel size of 0.945 μm/pixel. The slit sizes of the incident and diffracted X-rays were adjusted at every 2θ angle, to fix the Ge-SSD dead time at less than 15%. The EDXD patterns were analyzed using the software package provided by the beamline (Kono et al., 2014a) to obtain the structure factor S(q) and the reduced pair distribution function G(r), respectively. S(q) gives important information about the intermediate range ordering of the melt structure and through its Fourier transform G(r), distances between atom pairs might be determined. After EDXD acquisition was completed experiments were quenched by shutting down the power, then decompressed.

2.3. Chemical analyses and textural observations of the recovered quenched products

The recovered Paris-Edinburgh (PE) cells from the quenched runs were opened and the extracted capsules were embedded in epoxy resin and polished using ethanol to perform analyses to assess their chemical composition, textural features and, finally, spectroscopic properties. The recovered experimental products, all contained in a graphite capsule, were first observed under an optical microscope and showed the homogeneous surface of the quenched glasses (Fig. S1a-e of the Supplementary Materials). Textural observations were performed on carbon coated polished samples using the FEI QUANTA 400 scanning electron microscope available at the Department of Earth Sciences of Sapienza University (Rome). The chemical composition of the quenched products was analyzed using the electron microprobe (EMPA) Jeol JXA-8200 Superprobe available at Istituto Nazionale di Geofisica e Vulcanologia (INGV, Rome). An accelerating voltage of 15 kV, beam current of 7.5 nA and defocused beam with a diameter of 5 μm were employed as operating conditions. For an accurate chemical composition, the following standards were used: Albite (Na, Si, Al), Apatite (Ca), Forsterite (Mg), Tugtupite (Cl) and Pyrite (Fe). Given the peculiarity of our quenched glasses, EMPA and SEM analyses were additionally carried out for comparison at the Bayerisches Geoinstitut (BGI, Germany) using JEOL JXA-8200 and Zeiss Gemini 1530, and repeated at INGV only on samples CARB2_2_2016, CARB2_4 and CARB2_2_2018.

2.4. Micro-Raman spectroscopy

Raman spectra were collected on the polished samples after removal of the C coating using the Horiba LabRam HR 800 spectrometer available at the Department of Science of University of RomaTre (Italy). Data were collected with a 600 grooves/mm spectrometer grating and a CCD detector. A Nd-YAG laser at 532 nm (green laser) was used as the light source with 60 mW laser power, a confocal hole of 300 μm, slit size of 200 μm and an exposure time of 120 s. This long acquisition time was preferred in order to improve signal-to-noise ratio, but no changes were observed in terms of either peak intensity or Raman shift with respect to test measurements conducted with shorter acquisition times. The Raman scattering was collected by a 100× objective and ~ 5 μm^2 spot size on the polished sample surface over a range from 100 to 1800 cm^{-1} and from 2900 to 4200 cm^{-1} with a resolution of 1.8 cm^{-1}. Additional Raman spectroscopy measurements over the entire range 100–4000 cm^{-1} using both green (532 nm) and red (632.8 nm) lasers were also performed in order to have a more detailed characterization of these peculiar quenched products. Spectral frequency was calibrated using the incident laser line and a Si single crystal. An average of 4 measurements were performed on each sample to verify its spectroscopic homogeneity. The obtained spectra were processed to account for the temperature and excitation line effects (Long, 1977) and PeakFit© software for smoothing, baseline removal and deconvolution.

2.5. Micro-infrared spectroscopy at both ambient and high pressure

The polished glasses embedded in epoxy resin were analyzed by Fourier transform micro-infrared spectroscopy in reflection mode (μ-R-FTIR) at the Material Science branch of SISSI beamline of CNR-IOM at Elettra synchrotron in Trieste (Italy). The analyses were carried out in the region 600–6000 cm^{-1} using a Vertex 70v interferometer coupled with a Hyperion2000 microscope (Bruker Optics), a nitrogen cooled HgCdTe (MCT) detector and a KBr beam splitter. Measurements were conducted using a conventional thermal source (Globar) with a resolution of 1 cm^{-1} and an aperture of 80 μm by collecting three acquisitions per area of 128 scans each. The reflectance was determined with respect to a flat gold mirror as it reflects near 100% of light in mid IR, the spectrum of which was collected under the same experimental conditions. Only CARB2_4 sample was measured at the Department of Physics of Sapienza University in Rome using the Vector 22 Bruker interferometer equipped with a broadband MCT detector and a Globar infrared source coupled to the Hyperion 1000 infrared microscope. For this sample, the reflectance spectra were collected between 600 and 8000 cm^{-1} with a resolution of 2 cm^{-1} with respect to a flat silver mirror (~100% reflectivity in mid IR) using the same aperture from 50 μm × 50 μm to 200 μm × 200 μm in size. Three acquisitions of 128 scans each were performed on the selected area. In addition, transmission FTIR measurements (μ-T-FTIR) were conducted on 200 μm-thick double polished samples of CARB2_2_2016, CARB2_2_2018 and CARB2_4 at the Department of Physics of Sapienza University in Rome using a Vertex 70v interferometer coupled to the Hyperion 1000 infrared microscope. Sample spectra as well as background spectra were collected between 400 and 6000 cm^{-1} with a resolution of 2 cm^{-1}. Five acquisitions of 128 scans each were collected.

The vibrational properties of CARB2_4 glass were also investigated by μ-R- and μ-T-FTIR spectroscopy at HP and room T. A symmetric diamond anvil cell (DAC) was used for reflectance measurements coupled with the setup available at SISSI-Mat described above (Lupi et al., 2007; Piccirilli et al., 2012). A tiny chip of the glass (~70 μm of diameter) was loaded in the DAC equipped with low-fluorescence IIas-type diamonds with 500 μm culet diameter, an Inconel gasket 100-μm thick with a 200-μm drilled hole, and KBr powder (transparent in the mid IR range) used as pressure medium. A ruby sphere was placed near the glass chip as for in situ pressure calibration (Mao et al., 1986). Mid-IR spectra were acquired in the range of 600–6000 cm^{-1} with a resolution of 1 cm^{-1} and an aperture of 60 μm. Reflectance was calculated with respect to the intensity of Au corrected for the intensity reflected from the external face of the diamond. μ-T-FTIR measurements were carried out at SISSI-MAT beamline with a Belleville spring DAC (LotoEng company) 20 mm height equipped with low-fluorescence IIas-type diamonds with 300 μm culet diameter, an Inconel gasket 150-μm thick with a 150-μm drilled hole, using synchrotron light as source. Spectra were acquired in the range of 600–8000 cm^{-1} with a resolution of 2 cm^{-1} and an aperture of 30 μm using CsI as quasi-hydrostatic P medium (transparent in the mid IR range). The characteristic spectra of either sample or diamond or salt were all collected with three acquisitions of 128 scans each. Transmittance was calculated by dividing the spectra of the sample in the DAC with CsI by those of the DAC filled with CsI only, which accounts for background contributions. The collected raw spectra were, then, elaborated using both OPUS™ (version 8.2) and RefFIT softwares. Smoothing and deconvolution of the spectra were performed using PeakFit© software.

2.6. In situ Mössbauer analysis

The $Fe^{3+}/\sum Fe$ ratio of CARB2_4 glass (1.4 GPa/1815 °C) was determined at room T through in situ synchrotron Mössbauer source (SMS) spectroscopy at the ID18 Nuclear Resonance Beamline of the European Synchrotron Radiation Facility (ESRF; Grenoble, France). SMS technique exploits the (111) Bragg reflection of a $^{57}FeBO_3$ crystal, mounted on a Wissel velocity transducer and driven with a sinusoidal waveform, to obtain the Mössbauer characteristic energy of 14.4 keV (Potapkin et al., 2012). Kirkpatrick-Baez mirrors were used to focus the beam onto an area of about 5 × 15 μm^2. The velocity scale was set to ±6 (mm/s) and calibrated using a 25-μm thick α-Fe foil. Data collection required 8 h, considering that the glass was not ^{57}Fe enriched, with low FeO wt% (about 2.7 wt%). The spectrum was fitted by full transmission integral with a normalized pseudo-Voigt line-shape using the MossA software package (Prescher et al., 2012).

2.7. X-ray computed microtomography

X-ray computed microtomography (micro-CT) investigation was carried out on chips of samples CARB2_1 (2.6 GPa/1865 °C) and CARB2_4 (1.4 GPa/1815 °C) extracted from the C capsule using the Carl

Zeiss Xradia Versa-410 3D X-ray microscope available at the Istituto Nazionale di Geofisica e Vulcanologia-Sezione di Napoli "Osservatorio Vesuviano" (INGV-OV, Naples). The scan was performed over a 360° rotation using 1601 projections with a scan time of 18 s per projection, 40 kV voltage, and 3 W power with a spatial resolution of 1 μm/voxel.

3. Results

3.1. Liquid structure measurements at high pressure and temperature

We performed four successful measurements of the structure of carbonate-silicate liquids at P and T of 1.4 GPa/1815 °C (CARB2_4), 2.6 GPa/1865 °C (CARB2_1_2016), 4.3 GPa/1990 °C (CARB2_3_2016) and 4.4 GPa/1950 °C (CARB2_2_2016) (Table 1). It can be noted that these P-T conditions are slightly different from those at which the viscosity was determined (e.g., CARB2_2_2016 and CARB2_3_2016; Stagno et al., 2020a). In fact, during liquid structure measurements, it is preferable to set T slightly higher than the liquidus T at which viscosity measurements are conducted to prevent partial crystallization of the liquid sample caused by any electrical power fluctuation during the 3-h long acquisition time. The increase of T also causes a change of P. We consider the P_{fin} and T_{fin}, which are estimated just before quench (Table 1) as representative of the target experimental conditions of the structure data. The typical uncertainties for PE experiments at HP-T are less than 0.4 GPa and 60 °C, as discussed in Kono et al. (2014a, 2014b).

The EDXD diffraction patterns of the molten samples collected at the 2θ angle of 15.0161° just before data acquisition show their amorphous nature (some sharp peaks are from the graphite capsule, the surrounding ceramics and the WC anvils) at the investigated P-T conditions (Fig. S2a-d). Fig. 2 shows the structure factor, S(q), determined for the carbonate-silicate liquid at high P-T with values reported in Table 1 for the first sharp diffraction peak (FSDP; Elliott, 1991) of S(q). The differences among the patterns in Fig. 2 for each run can be explained as a result of P-T and composition. The position of the first sharp diffraction peak (FSDP; Elliott, 1991) in the structure factor S(q) was determined by Gaussian fitting and it varies from 2.13 $Å^{-1}$ at 1.4 GPa/1815 °C to 2.25 at 4.3 GPa/1990 °C, showing a positive dependence with increasing the P and T. The FSDP, except for the spectrum at 4.3 GPa and 1990 °C, shows a shoulder at about 1.5–1.8 $Å^{-1}$. A second peak appears at ~3 $Å^{-1}$, corresponding to the second sharp diffraction peak (SSDP; Elliott, 1995). The Fourier transformation of S(q) gives the reduced pair distribution function, G(r), by which information about interatomic distances of T-O (T = Si, Al, Fe^{3+}), T-T and M-O (M = Mg, Fe^{2+} and Ca) are usually determined. Here, conversely to studies conducted on either pure carbonate or silicate melts (e.g. Kono et al., 2014a; Hudspeth et al., 2018; Sakamaki et al., 2013; Wang et al., 2014), the chemical composition of the carbonate-silicate melt hampers the possibility to clearly distinguish such local structure of T (i.e., Si, Al and Fe^{3+}) and M (i.e., Mg, Ca, Fe^{2+}). This can be observed in Fig. S3 where the peak visible at 1.83–2.11 Å is indicative of both T-O and M-O contributions, the distinction of which is not straightforward given the complex composition of the melt investigated.

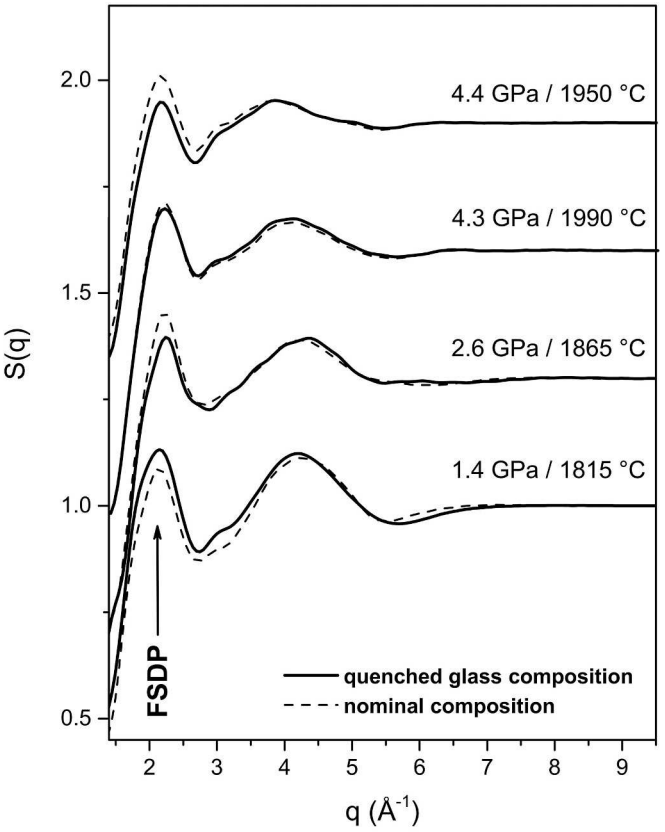

Fig. 2. Structure factor S(q) for CARB2 runs investigated by multi-angle energy dispersive X-ray diffraction at high pressure and temperature. Black lines refer to data processed using the composition of the quenched glasses (Table 2), while black dashed lines are representative of data processed using the nominal composition of the starting material. No significant differences are observed.

Table 1
Experimental conditions for HP-HT liquid structure measurements and obtained structural data, determined processing EDXD data using the composition of recovered quenched glasses.

Run	*$P_{initial}$ (GPa)	*P_{final} (GPa)	*$T_{initial}$ (°C)	*T_{final} (°C)	FSDP ($Å^{-1}$)	η_{calc} (Pa·s)
CARB2_1_2016	2.8	2.6	1870	1865	2.25 *(2.23)*	0.0553
CARB2_2_2016	2.6	4.4	1990	1950	2.20 *(2.18)*	0.0414
CARB2_3_2016	4.5	4.3	2012	1990	2.25 *(2.23)*	0.0351
CARB2_4	1.3	1.4	1815	1815	2.13 *(2.15)*	0.0660

Notes: FSDP values in brackets refer to positions determined processing EDXD data using the nominal composition of the starting material, the uncertainty of which is discussed in detail by Kono et al. (2014a). Viscosities are calculated after data from Stagno et al., 2020a as discussed in Section 4.1 and Supplementary Materials. *Typical uncertainties on pressure and temperature in the Paris-Edinburgh cell experiments are less than 0.4 GPa and 60 °C (e.g., Kono et al., 2014a, 2014b; De Grouchy et al., 2017; Hudspeth et al., 2018).

EDXD data were processed taking into account the chemical composition of the retrieved quenched glasses after the experiment (Table 2, see Figs. S4-S7 for additional information on data treatment). To assess any effect on structural parameters given by a variation in the melt chemical composition, we additionally processed data using the nominal composition of the starting material (Figs. S8-S11). The slight variations in S(q) between the two sets of data result in a negligible shift of the FSDP of ±0.02 Å, as reported in brackets in Table 1 and shown in Fig. 2 (dashed lines).

3.2. Chemical composition of the quenched glasses

The chemical composition of the five quenched glasses is reported in Table 2 with the P-T conditions at which the liquid structure measurements were carried out. Run CARB2_2_2018 is a glass recovered from a failed EDXD measurement. Photos taken under the optical microscope of the polished quenched glasses are reported in Fig. S1a-e. BSE images (Fig. S12a-e) show a vesicular glassy exposed sample surface. The chemical composition of the quenched products determined by EMP analysis varies from 18.75 to 30.91 wt% of SiO_2, 2.41 to 3.74 wt% of Al_2O_3, 28.06 to 41.47 wt% of MgO, 1.32 to 5.25 wt% of FeO, 9.82 to

Table 2
Chemical composition employed in the synthesis of CARB2 and results of EMPA analysis (INGV) on glasses quenched from HP-T experiments.

Oxides/samples	CARB2 nominal	CARB2_1_2016	CARB2_2_2016	CARB2_3_ 2016	CARB2_4	CARB2_2_2018
No. points analyzed	–	14	6	8	12	6
Quench P/T conditions	–	2.6 GPa 1865 °C	4.4 GPa 1950 °C	4.3 GPa 1990 °C	1.4 GPa 1815 °C	2.6 GPa 1735 °C
SiO_2	18.28	23.09(47)	18.75(9)	22.02(50)	30.91(45)	24.95(73)
Al_2O_3	1.95	2.87(13)	2.41(7)	2.93(11)	3.74(13)	3.47(5)
FeO	6.72	1.57(06)	2.28(18)	1.32(10)	2.76(8)	5.25(6)
MgO	27.50	30.09(35)	28.06(27)	32.39(67)	41.47(21)	31.05(51)
CaO	20.43	15.79(13)	14.86(23)	16.71(28)	9.82(25)	15.55(30)
Na_2O	1.37	0.64(11)	0.35(8)	0.77(7)	0.14(10)	0.79(36)
Cl^-	1.21	6.35(33)	5.55(27)	4.80(13)	4.42(39)	4.98(70)
Vol	22.54*	*19.54*	*27.72*	*18.99*	*6.68*	*13.09*
Total	100.00	80.46(62)	72.28(73)	81.01(94)	93.32(54)	86.90(43)

Notes: values in brackets indicate 1-sigma uncertainty. *CO_2 value of the starting material. Vol stays for the (C-O-H) volatile component dissolved in the quenched glass.

16.71 wt% of CaO, 0.14 to 0.79 wt% of Na_2O, 4.42 to 6.35 wt% of ClO^-. As a first approximation, the low totals (72.28–93.32 wt%) would indicate the presence of CO_2 that is lower than the CO_2-rich starting material (22.54 wt% CO_2) except for sample CARB2_2_2016 (27.72 wt% CO_2). Such variation might result from the variable P-T conditions at which the liquids were exposed. On the other hand, Fig. S12a-e does show the occurrence of secondary graphite laths (other than the primary source of graphite, the capsule) along with (pseudo-)spherical vacuoles some of which are filled to suggest possible liquid unmixing of a calcitic component (see Supplementary Materials). These textural observations along with the tomographic images collected on samples CARB2_1 and CARB2_4 (see Movie in SM), showing the absence of exsolved gas bubbles, provide evidence of the CO_2 undersaturation conditions at the time of quench. Additional EMPA analyses conducted at INGV and BGI (Tables S1 and S2) confirm the chemical composition of the recovered quenched products with no evidence of the presence of undesired contaminants revealed by SEM.

The lower FeO_{tot} content observed in the quenched glasses (1.32–5.25 wt%) compared with that of nominal CARB2 (6.72 wt%) is due to the alloying with the falling Pt sphere (up to about 40 wt% of Fe) occurring during the duration of the liquid structure measurements (see Supplementary Materials), well after the descent of the Pt sphere for viscosity measurements. The content of CaO also decreased by ~5 wt% (~11 wt% in CARB2_4; see Table 2) with respect to the nominal composition as a result of the segregation of some Ca-rich blobs of few microns in size formed during quench and surrounded by a Cl-rich thin halo (Fig. S12). In turn, a slight increase of SiO_2 is observed by ~4 and 5 wt% in run CARB2_1_2016 and CARB2_3_2016, respectively, and up to 12 wt% in CARB2_4. Interestingly, the high MgO content (41.47 wt%) of CARB2_4 glass is closely representative of carbonate-silicate magmas expected to form by melting of a carbonated harzburgite (Brey et al., 2008; Stagno and Frost, 2010; Girnis et al., 2011). As can be noticed in Table 2, the thin additional layers of $CaCO_3$ (run CARB2_1_2016) and San Carlos olivine+Li_2CO_3 (run CARB2_2_2018) inserted in the experimental capsule for viscosity measurements did not result in any significant changes in chemical compositions of these quenched glasses when compared to the others with no additional layer. Despite the change in composition with respect to the nominal composition, our glasses fall in the field between carbonatites and natural kimberlites (Fig. 1), for which spectroscopic properties are unexplored.

3.3. Raman spectra of quenched glasses

Large pockets of homogenous whitish glass with dimensions of at least 10 μm x10 μm are well distinguishable and exposed at the surface in all quenched glasses allowing the collection of confocal micro-Raman spectra on three samples CARB2_2_2016, CARB2_4 and CARB2_2_2018. The other two samples (CARB2_1 and CARB2_3) could not be measured because of high fluorescence. The entire Raman spectra of the glasses along with the spectrum of the employed epoxy resin in which experimental capsules were embedded are shown in Figs. S13-S15 of the Supplementary Materials. We observed no differences between spectra collected using green laser and red laser. These are characterized by bands distributed within two main regions of 700–1200 cm^{-1} and 3100–3700 cm^{-1}. In addition, Raman spectra of CARB2_2_2016 and CARB2_4 glasses show small peaks arising in the region 2050–2150 cm^{-1}. Spectra of carbonate-silicate glasses in the low frequency region are characterized by broad overlapped bands ranging from 850 to 1100 cm^{-1}. These broad peaks arise from T-O stretching vibrations of Q_n-species, where *n* refers to the number of bridging oxygens distributed among SiO_4 and AlO_4 units. The peak at 720 cm^{-1}, plus a minor contribution at 790 cm^{-1} in CARB2_2_2016 (Figs. S13-S15), has also been assigned to the Si-O stretching (translational) mode according to Matson et al. (1983). Given the composition of the starting material employed in this study, such convoluted bands are expected to contain also a contribution from the ν_1 symmetric stretching vibration of CO_3^{2-} as it falls in this frequency range, too. Vibrations in the region 2050–2150 cm^{-1} (Fig. S16) were attributed to carbon monoxide (Yoshioka et al., 2015, 2019; Armstrong et al., 2015; Grewal et al., 2020) both free and likely bonded to either Fe or Pt atoms to form carbonyls. The 3100–3700 cm^{-1} interval is visible in runs CARB2_2_2016 and CARB2_2_2018 and assigned to the presence of OH bonds, which can be associated with the presence of either hydroxyl groups (OH) or molecular H_2O. The amount of dissolved H_2O was determined using the procedure proposed by Le Losq et al. (2012) that results in H_2O content of 0.41 wt% and 0.16% wt% for CARB2_2_2016 and CARB2_2_2018, respectively. Similarly, the model proposed by Di Genova et al. (2017) results in 0.54 and 0.43 wt% H_2O.

Fig. 3a-c shows the deconvoluted spectra at 800–1150 cm^{-1} after correction for the temperature and excitation line effects using the equation proposed by Long (1977), smoothing and baseline subtraction using a cubic-spline line (anchor points at ~650, 785, 1150 cm^{-1}). The best fit to our spectra was obtained using 5 peaks according to the vibrational modes as in Moussallam et al. (2016), representative for ν_s Si-O in Q_0, Q_1, Q_2 silicate units + one peak for vibrations involving bridging oxygen atoms in any Q_n (ν_s Si-BO in Q_n, hereinafter referred as Si-O^0; Mysen et al., 1982, Le Losq et al., 2015) and one for ν_1 CO_3^{2-}. The initial peak position and width were both left free to adjust until the optimal R^2 value was reached. All spectra show a peak at ~860 cm^{-1} corresponding to Q_0 increasing in intensity from CARB2_2_2016 (2.41 wt% Al_2O_3) to CARB2_2_2018 (3.47 wt% Al_2O_3) and more intense in CARB2_4 (3.74 wt% Al_2O_3). These are followed by a peak at 880 cm^{-1} relative to Q_1 and at 950 cm^{-1} (940 cm^{-1} in CARB2_2 2018) representative of Q_2. A peak at about 1020 cm^{-1} corresponding to Si-O^0 appears as a shoulder to the dominant peak at 950 cm^{-1} observed in all compositions. A deconvoluted peak at 1081 cm^{-1} is observed in CARB2_2 2016 (27.72 wt% CO_2) and a distinct peak in CARB2_2 2018 (13.09 wt% CO_2) at 1092 cm^{-1}, both attributable to ν_1 CO_3^{2-} rather than any Q_3

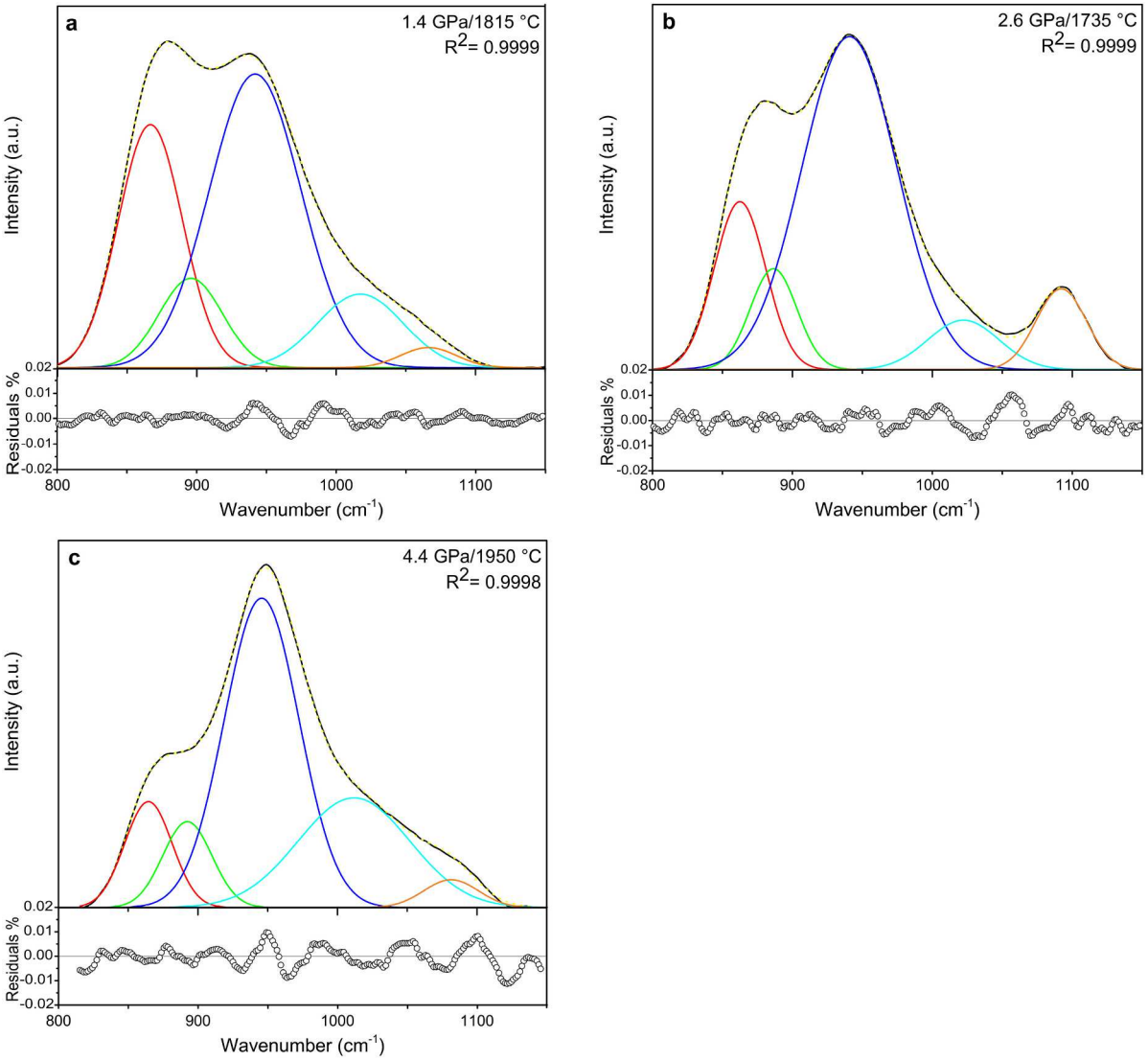

Fig. 3. Deconvoluted Raman spectra for runs CARB2_4 (a), CARB2_2 2018 (b) and CARB2_2_2016 (c). Red, green, blue, light blue and orange fitting curves are for Q_0, Q_1, Q_2, Si-BO (see text) and ν_1 carbonate stretching, respectively. (For interpretation of the references to colour in this figure legend, the reader is referred to the web version of this article.)

species of aluminosilicate units due to the weakly polymerized nature of our glasses. In CARB2_4 (6.68 wt% CO_2) this peak is less visible at 1066 cm^{-1}. No evidence of molecular CO_2 is observed in any of the three quenched glasses. Additional information of peak position, FWHM and area% are available in Supplementary Materials.

3.4. *μ-R- and μ-T-FTIR spectroscopy of the quenched glasses at ambient pressure*

μ-R-FTIR spectra were collected from the quenched glasses listed in Table 2 embedded in epoxy resin. The full spectra are shown in Fig. S17 of the Supplementary Materials in the whole range of acquisition from 600 to 6000 cm^{-1}, with the main features being visible within the 600–1500 cm^{-1} and 3000–4000 cm^{-1} regions. The assigned bands are after King et al. (2004) and Grzechnik et al. (1996). From the whole collected spectra, a mode at 660–695 cm^{-1} arises and was associated to bending vibrations of C-O in CO_3^{2-}. Then, an intense broad band is observed at 940–980 cm^{-1} that is related to the Si-O and Al-O asymmetric stretching vibrations in tetrahedral TO_4-T_2O_7-TO_3 orthosilicate-pyrosilicate-metasilicate units. The doublet at ~1210–1380 cm^{-1} is representative of the ν_3 asymmetric stretching vibrations of carbonate groups, and results in an increase of the splitting ($\Delta\nu_3$) from 121 cm^{-1} (CARB2_4) to 165 cm^{-1} (CARB2_2_2016), which appears to be correlated to the dissolved volatile content. In addition, the carbonate doublet appears asymmetric, with the peak at lower wavenumber being more intense from 1.4 GPa/1815 °C (run 4) to 4.4 GPa/1950 °C (run 2_2016) and 4.3 GPa/1990 °C (run 3_2016). No evidence of molecular CO_2 is observed in any of the FTIR spectra obtained. The presence of the band near 3550 cm^{-1} is representative of H_2O_{tot} that likely entered the sample during the experiment of melt structure or during the loading of the capsule.

From each spectrum the absorption coefficient (α) of the carbonate-silicate glasses as a function of frequency was determined using the following equation,

$$\alpha(\nu) = 4\pi\nu k \quad (1)$$

where ν is the frequency in cm^{-1} and k the imaginary part of the refractive index calculated along with the real part, n, (McMillan, 1985) using the Krames-Kronig (KK) transformation of reflectance data as part of the OPUS™ software package. Fig. 4a-e displays the absorption coefficient α in the region 800–1550 cm^{-1} derived from KK transformation of reflectance spectra, after baseline correction, smoothing and

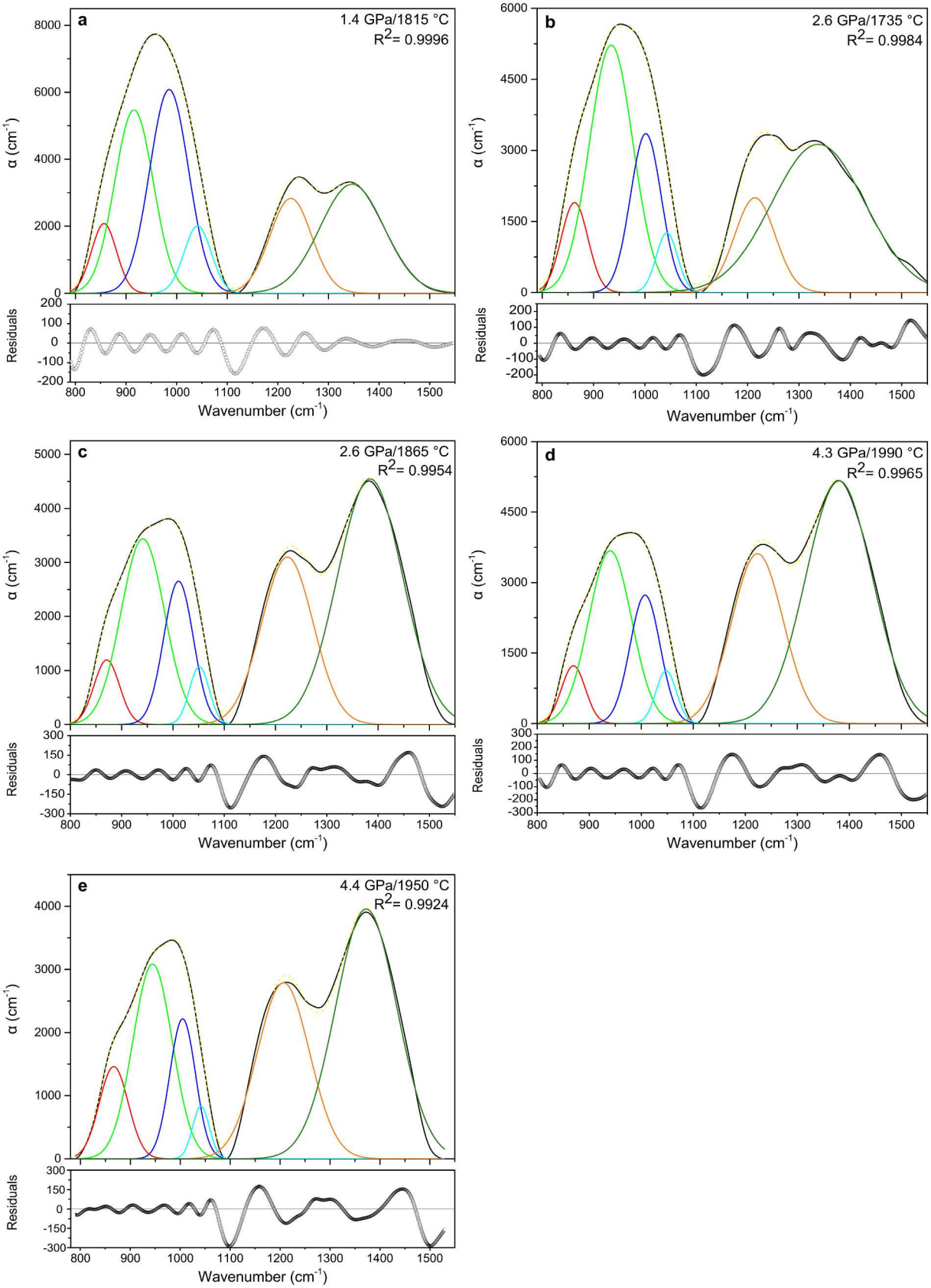

Fig. 4. Deconvoluted FTIR spectra with absorption coefficient α calculated from reflectance data using the Kramers-Kronig analysis. Red, green, blue lines correspond to Q_0, Q_1, Q_2 species, respectively. The other lines correspond to carbonate vibrations ν_1 (light blue) and ν_3 doublet (orange and dark green lines). (For interpretation of the references to colour in this figure legend, the reader is referred to the web version of this article.)

deconvolution. We employed 6 peaks positioned at ~860 cm^{-1}, 910 cm^{-1}, 960 cm^{-1}, 1040 cm^{-1}, 1220 cm^{-1}, 1360 cm^{-1} taking as reference literature data (Piriou and Arashi, 1980; McMillan and Wolf, 1995; Genge et al., 1995; King et al., 2004; Wilding et al., 2019) to account both for the silicate and carbonate contributions. Peak parameters were not constrained during iteration to achieve the best R^2 value. Results from the deconvolution procedure carried out in the silicate region for CARB2 glasses show the four peaks centered between 856 and 871 cm^{-1} (I), 916–944 cm^{-1} (II), 985–1011 cm^{-1} (III), 1041–1051 cm^{-1} (IV), 1207–1226 cm^{-1} (V), 1337–1384 cm^{-1} (VI). We assign bands I-III to the asymmetric stretching vibrations of Q_n tetrahedral units in TO_4 units (Q_0 species), T_2O_7 (Q_1 species) and TO_3 units (Q_2 species), respectively. The band IV was assigned to ν_1 symmetric stretching of CO_3^{2-}. Bands V and VI were assigned to the ν_3 asymmetric stretching vibrations of the carbonate doublet. A shift to higher wavenumbers is observed for the silicate bands I, II and III as a function of decreasing $SiO_2 + Al_2O_3$ content and increasing volatile content (Table 2), whereas the opposite trend is observed for band V.

The μ-T-FTIR spectra were acquired on double-polished, 200 μm-thick samples CARB2_2_2016, CARB2_4, CARB2_2_2018. Transmittance spectra are shown in Fig. 5 to underline the saturation (i.e, transmittance value equal to zero) observed from 400 to 1600 cm^{-1}, therefore testifying the carbonated nature of the quenched glasses.

In order to visualize the carbonate bands, the quenched glasses were required to be double polished to quite low thickness. However, the combination of μ-T-FTIR to μ-R-FTIR allowed the successful resolution of this spectral region as illustrated previously.

Consistent with that which is observed by Raman spectroscopy in Fig. S16, the 2000–2100 cm^{-1} region shows vibrations at 2022, 2041, 2050, 2062 and 2087 cm^{-1} (Fig. 6) in CARB2_2_2016 and CARB2_4 (some occurring as a shoulder in the latter). Those peaks are assigned to C-O stretching vibrations associated with carbonyl groups bonded to a transitional metal (Xu, 2002 and references therein). Further, a peak at 2210 cm^{-1} attributed to free molecular carbon monoxide (Eggler et al., 1979; Brooker et al., 1998, 1999; Stanley et al., 2014; Armstrong et al., 2015; Yoshioka et al., 2015, 2019) is observed in all three samples investigated, which is shifted with respect to the fundamental vibration of gaseous CO at 2143 cm^{-1} as CO is dissolved in the glass matrix, in agreement with results reported in the aforementioned studies.

All three of the investigated samples show absorptions in the 3000–3700 cm^{-1} region (Fig. 5), which is relative to O-H stretching. CARB2_2_2016 shows more pronounced peaks at 3265 and 3355 cm^{-1}. An estimation of dissolved H_2O_{tot} from transmission measurements of the quenched glasses is proposed by applying the Lambert-Beer law using a range of values of extinction coefficients available in literature for mafic glasses, which vary from 59 to 68 L/mol·cm (Shishkina et al., 2014 and references therein) and a density interval of 2300 g/L (Ghosh and Karki, 2017) and 2600 g/L. Our estimation of H_2O_{tot} yielded values comprised between 0.2 and 0.3 wt% for CARB2_2_2016 and 0.5–0.6 wt % for CARB2_4. As it can be observed in Fig. 5, the transmission spectra collected for CARB2_2_2018 show saturation also in the O-H region. Therefore, based on our data we can estimate a H_2O_{tot} content which is expected to be slightly higher than 0.8–1 wt% for CARB2_2_2018 glass. It is worth noting that it is extremely difficult to keep these systems dry, as inferred by Weidendorfer et al. (2020). However, it is likely that such low amount of water only has a negligible effect on both viscosity and liquid structure considering their depolymerized nature.

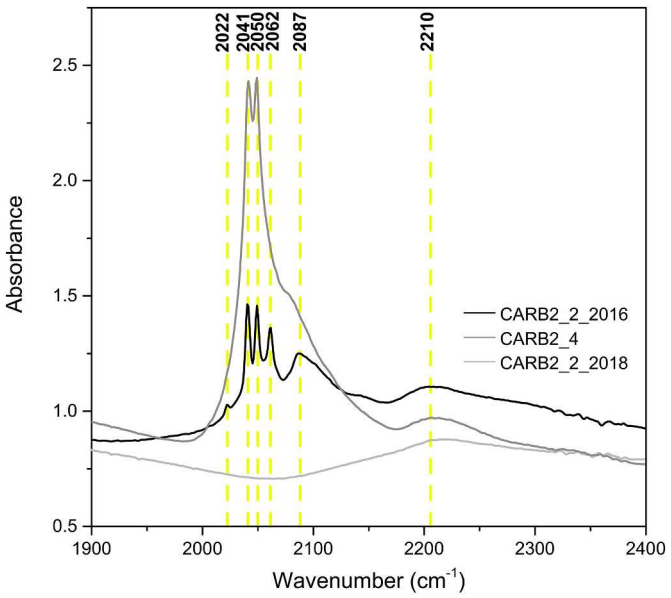

Fig. 6. Absorbance spectra of CARB2 quenched glasses showing peaks attributed to metal carbonyl complexes in CARB2_2_2016 and CARB2_4 at 2022, 2041, 2050, 2062 and 2087 cm^{-1}, along with free carbon monoxide (2210 cm^{-1}) which is instead present in all of the three quenched products.

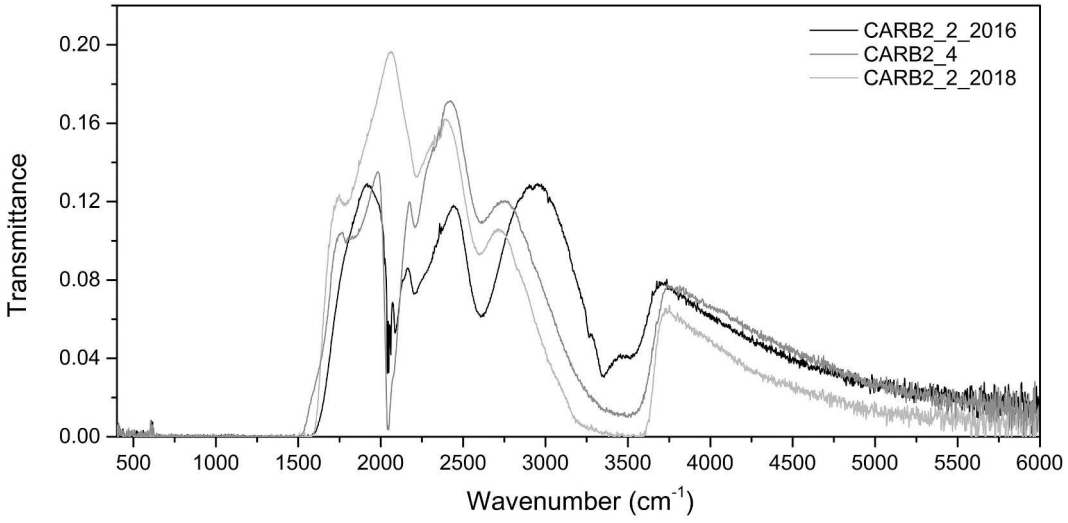

Fig. 5. Mid-infrared transmission spectra of recovered CARB2_2_2016, CARB2_4 and CARB2_2_2018 glasses collected at ambient pressure and room temperature conditions.

3.5. μ-R-FTIR and μ-T-FTIR spectroscopy of a carbonate-silicate glass at high pressure

The effect of P was investigated on chips of transparent glass extracted from sample CARB2_4. Spectra were collected in reflection mode during compression up to 5.6 GPa and decompression and analyzed for changes both in peak intensity (reflectance) and spectral shift. A procedure similar to that adopted for ambient P spectra was employed in order to better understand each specific contribution arising both from carbonate and silicate vibrations. Refractive indexes were obtained from the reflectance spectra taking into account the effect of diamond. Then, absorption coefficients were calculated using Eq. (1), and the same procedure as for quenched glasses in air was adopted. Fig. 7 shows the absorption coefficient, α, calculated from reflectance spectra (with Au used as reference) after removal of sample-diamond interface contribution. The ambient P spectrum shows a broad band in the spectral regions 800–1160 cm^{-1} associated to silicate modes, and an absorption doublet around 1180–1270 cm^{-1}, we associated to carbonates. Lower pressure spectra show two evident peaks at 970 cm^{-1} and 1030 cm^{-1} composing the band. When pressure is increased, the peak at 1030 cm^{-1} becomes more intense, as can be observed from spectra collected at 2.4, 4.1 and 5.6 GPa, possibly causing the gradual blueshift of the whole band to 1090 cm^{-1}. This shift is reversible upon decompression as can be seen in Fig. 7; while a negligible variation is observed for the carbonate doublets. To achieve a quantitative structural evaluation, we used a deconvolution procedure based on peaks assignment described above. Importantly, an additional peak placed at 1080–1100 cm^{-1} was necessary to fit all spectra (Fig. S18), in contrast with those at ambient P discussed above. This peak was attributed to the formation of Q_3 species for increasing pressure at room T. The position of the first peak shows no significant spectral shift with increasing P, the second peak was observed to shift from 911 cm^{-1} to 916 cm^{-1} with increasing P and from 915 cm^{-1} to 906 cm^{-1} upon decompression. The carbonate doublet shifts to lower wavenumbers with respect to ambient-P data upon compression with the peaks varying from 1188 to 1180 cm^{-1} and from 1270 to 1255 cm^{-1} up to 4.1 GPa. At 5.6 GPa the doublet shifts to higher frequencies as 1196 and 1260 cm^{-1}. In addition, the splitting between the two peaks decreases from 82 to 64 cm^{-1} with increasing P.

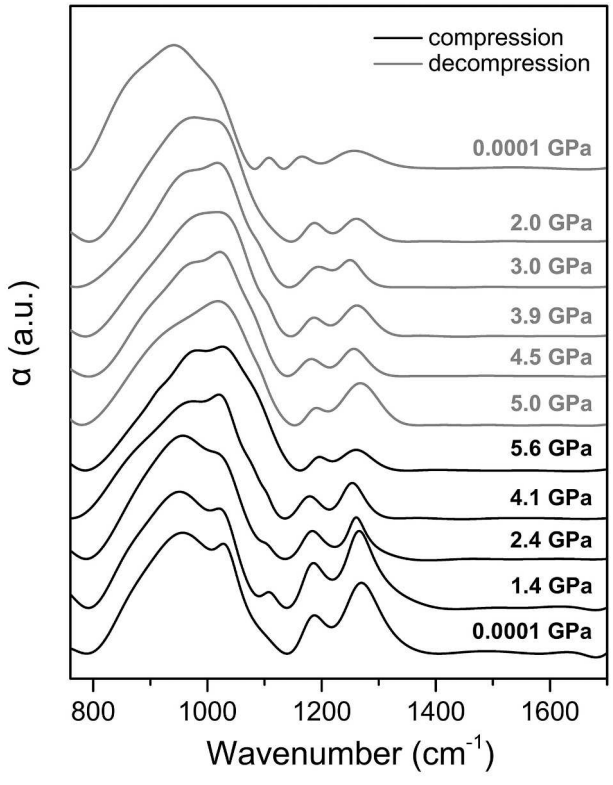

Fig. 7. The absorption coefficient α calculated from reflectance FTIR spectra collected upon compression and decompression on CARB2_4 glass at room T and high P.

Spectra relative to in situ HP μ-T-FTIR investigation of CARB2_4 glass chip from 0.8 up to 11.1 GPa are shown in Fig. S19, as well as that of the retrieved decompressed sample. In these spectra peaks at ~720, 1080, 1460, 2900, 4250, 4320, 5680 5780 cm^{-1} can be distinguished. These peaks were assigned to CO_3^{2-} vibrations (e.g. Genge et al., 1995), further confirming the high carbonate content of the quenched glasses. Specifically, CO_3^{2-} ν_4 bending is observed at 720 cm^{-1}, 1080 cm^{-1} band was assigned to ν_1 stretching and 1460 cm^{-1} to ν_3 stretching, with overtones $2\nu_3$, $3\nu_3$ and $4\nu_3$ at 2900 cm^{-1}, 4250 and 4320 cm^{-1}, 5680 and 5780 cm^{-1}, respectively. These peaks show saturation in transmission up to 2900 cm^{-1} (Fig. S19a), hindering the possibility to precisely determine band positions and how these vary during compression at room T, as well as to resolve ν_3 stretching doublet (i.e. it appears as one band only), which is instead visible for CO_3^{2-} $3\nu_3$ and $4\nu_3$ overtones (Fig. S19c). The region 1800–2700 cm^{-1} is hidden by diamond anvils, therefore covering any free CO and/or carbonyl contributions which were instead observed at aP (Figs. 6 and 7). As P is increased, a blueshift occurs for all bands (Fig. S19 b, c), accompanied by broadening.

3.6. Iron oxidation state of carbonate-silicate glass

The $Fe^{3+}/\sum Fe$ of CARB2_4 was determined by in situ SMS spectroscopy. The choice of this quenched glass was motivated by the marked spectral features of carbonyls (i.e., higher peak intensity) and, therefore, the possibility to investigate a possible redox mechanism involving the fluid species and the liquid at high P and T. The collected spectrum was fitted with two symmetric doublets, one for Fe^{2+} and one for Fe^{3+} (Fig. S20). The hyperfine parameters used for the fitting, quadrupole splitting (QS), central shift (CS) and full width at half maximum (FWHM) are reported in Table S3 and are compatible with literature data for basaltic glasses (e.g., Partzsch et al., 2004; Blundy et al., 2020). The contribution of Fe from the confocal Be-lenses, a component of the beamline set-up, was constrained by fitting the spectrum with an extra singlet (CS = 0.2991 mm/s; FWHM = 0.5694), based on preliminary background measurements. The $Fe^{3+}/\sum Fe$ ratio resulted in 0.14 ± 0.03, which is lower than what was expected in the case of CO_2-bearing oxidized liquids (and glasses).

4. Discussion

4.1. The structure of CO_2-bearing melts with implications for magma viscosity

Table 1 shows the position of the FSDP from structure factors determined from EDXD measurements at different P/T conditions. The structural investigation conducted by EDXD at high P and T showed that carbonate-silicate liquids are characterized by a shift in the FSDP position in reciprocal space towards higher values as a result of the combined effect of increasing both P and T. As a consequence, the intermediate range order (IRO = $2\pi/q_{FSDP}$) of carbonate-silicate liquids undergoes a shrinkage (from 2.95 Å to 2.79 Å), in agreement with observations for molten calcite (Hudspeth et al., 2018), melilititic liquids (Stagno et al., 2020b) and silicate liquids with different degrees of polymerization (e.g. diopsidic and jadeitic liquids discussed by Wang et al., 2014). In contrast, the position of the FSDP extrapolated from the structure factor reported for MORB liquids by Sakamaki et al. (2013) gives a negative correlation as a function of P (and T), peculiar among silicate compositions. This behavior moreover is opposite to that observed upon cold compression for glasses with similar composition (Ohashi et al., 2018).

Our results allow exploration of the dependence of the viscosity of

carbonate-silicate liquids at high P-T on their structure and compare this with the data available for calcite (Kono et al., 2014b; Hudspeth et al., 2018), MORB (Sakamaki et al., 2013) and melilititic liquids (Stagno et al., 2020b). Viscosity data for carbonate-silicate liquids (Stagno et al., 2020a) were fitted using a Non-Arrhenian Vogel-Fulcher-Tammann (VFT) equation modified to account for the effect of pressure as in Ritter et al. (2021), details can be found in Supplementary Materials.

Fig. 8 shows the viscosity calculated at the P and T at which the FSDP is measured for each composition. Calcitic liquids are characterized by a constant viscosity over the range of FSDP suggesting that variations in the medium range order such as shrinkage and packing of the carbonate molecules does not necessarily imply changes in the transport properties of these melts. In contrast, the incorporation of Si atoms represented by carbonate-silicate liquids contributes to the increase of polymerization accompanied by an increase in viscosity. Liquids with 22–30 wt% SiO_2 are characterized by viscosities up to 1 order of magnitude higher with respect to calcitic (but also dolomitic) liquids. The increase of SiO_2 (and Al_2O_3) in the melilititic liquid (Stagno et al., 2020b) causes the viscosity to further increase. Because T acts to stretch out the Si(Al)-coordinated polyhedra, the polymerized network undergoes relaxation associated with a viscosity decrease. In the case of carbonate-silicate and foiditic liquids, the decrease in IRO also causes the viscosity to decrease, a behavior that appears opposite to that observed in the case of more polymerized MORBs (Sakamaki et al., 2013).

These experimental observations raise important considerations on whether the viscosity of CO_2-bearing magmas at upper mantle P-T conditions should be treated by taking into account the amount of dissolved carbonate versus SiO_2 (Morizet et al., 2017b) or by implementing available current models that take into account also the melt structure as function of P-T and chemical composition.

4.2. *Vibrational properties of carbonate-silicate glasses from high P-T experiments with implications for carbon speciation in the upper mantle*

The sparse reflectance FTIR data for CO_2-bearing silicate glasses differ strongly from the glasses investigated in this study. Basanitic and leucititic glasses (Grzechnik et al., 1996), rhyolitic glasses (Moore et al., 2000), and melilititic glasses (Stagno et al., 2020b) are all characterized by two main regions of Si(Al)-O stretching vibrations (900–1100 cm^{-1}) and molecular/ionic C (CO_2, 2350 cm^{-1}, CO_3^{2-}, ~1300–1500 cm^{-1}). Features in the silicate region shift to lower wavenumber by increasing the CO_3^{2-} content into the melt as a result of depolymerization of the silicate network. Our spectra are characterized by silicate peaks at even lower frequencies than those reported by the aforementioned literature, which denotes the extreme depolymerized nature of these carbonate-silicate glasses. As far as the fingerprint relative to the carbonate anion is concerned, we observe a strong influence of the chemical composition in the vibrational properties of ν_3 asymmetric stretch of CO_3^{2-} where α (here indicated in terms of midpoint) decreases in wavenumber from ~1480 cm^{-1} in leucite-basanite glasses (Grzechnik et al., 1996) to 1315 cm^{-1} and 1306 cm^{-1} in melilititic glasses (Stagno et al., 2020b) to about 1300–1285 cm^{-1} as observed for carbonate-silicate glasses in this study. Such a marked shift was neither reported in the reflectance spectra of SiO_2-free carbonate-rich glasses (Genge et al., 1995) nor in previous studies carried out in transmission mode (Moussallam et al., 2016). Importantly, the dependence of the shift to lower wavenumbers of the carbonate doublet from the chemical composition is also accompanied by an increase in doublet splitting, which varies from ~90 cm^{-1} (leucite basanite glasses, Grzechnik et al., 1996) to 130 cm^{-1} and 140 cm^{-1} for melilititic glasses (Stagno et al., 2020b) up to 165 cm^{-1} in the compositions investigated in this study (Fig. 4). The increase in doublet splitting is related to an increase in the degree of distortion of CO_3^{2-} from the ideal trigonal planar symmetry (e.g. Blank and Brooker, 1994; Brooker et al., 2001b). In contrast to the Raman spectra, the reflectance spectra and the derived absorption coefficients clearly show the increase of the relative intensity between carbonate and silicate groups as the CO_2 content increases. In particular, the spectra taken on glasses CARB2_1 and CARB2_2_2016 present the carbonate doublets (ν_3) more pronounced with respect to the silicate group, opposite to what has been observed by Raman spectroscopy where the contribution of ν_1 stretching of CO_3^{2-} appears to be weak with respect to the silicate vibrations. Noteworthy, this ν_1 stretching vibration was also identified in our reflectance data (1040-1051 cm^{-1}), along with the bending vibration of C-O in CO_3^{2-} (660–695 cm^{-1}), which becomes more and more pronounced with increasing volatile content as determined from EMPA totals (Fig. S17).

The coexistence of CO_3^{2-} with CO (either interpreted as free CO or CO linked to a transition metal, i.e. Fe) was previously observed in studies of the CO solubility in silicate melts and the speciation of C species as a function of oxygen fugacity (Eggler et al., 1979; Brooker et al., 1998, 1999; Stanley et al., 2014; Armstrong et al., 2015; Yoshioka et al., 2019). The FTIR peak located between ~2100–2200 cm^{-1} has been previously assigned to free CO present in glasses (e.g. Eggler et al., 1979; Brooker et al., 1998, 1999), whereas Wetzel et al. (2013) and Stanley et al. (2014) proposed the formation of Fe-carbonyl complexes. Later works (Yoshioka et al., 2015, 2019) stressed that such peaks occurring around 2110 cm^{-1} in Raman spectra and 2210 cm^{-1} in FTIR spectra still appeared in CO-bearing Fe-free glasses, questioning their attribution to Fe-carbonyls. Metal carbonyl absorption bands usually occur between 1800 and 2100 cm^{-1}, with the position depending on the bonding mode (e.g., terminal, metal-CO, or bridging, metal-CO-metal), metal involved and electron density (Zhou et al., 2001; Socrates, 2004). Considerable literature on CO adsorption on metals, metal oxides and halides as well as zeolites (as reviewed by Xu, 2002) showed that a key feature of carbonyls is a band centered between 2100 and 2000 cm^{-1} made of a series of infrared absorptions (~4) occurring with an interval of 10–35 cm^{-1} one from another. Studies from various fields are helpful on pointing out that the different compounds present in the system under investigation play a role in determining the position of peaks with respect to those of metal carbonyls alone. For instance, Hugues et al. (1982) investigated the effect of $Fe_3(CO)_{12}$ and $Fe(CO)_5$ adsorbed on SiO_2, Al_2O_3 and MgO, revealing bands at 2013, 2033, 2053, 2110 cm^{-1} in the case of SiO_2, 2008, 2020, 2082 cm^{-1} on hydrated Al_2O_3, 2010 and 2078 cm^{-1} on MgO. Trusheim and Jackson (1983) investigated SiO_2-adsorbed $Fe(CO)_5$ finding peaks at 2002 and 2024 cm^{-1} and $Fe(CO)_5$ coexisting with $Fe_3(CO)_{12}$ under certain conditions, identified from a peak at 2052 cm^{-1}. Brandt et al. (1993) studied CO adsorbed on Pt/SiO_2 determining absorptions at 2065, 2080, 2087 cm^{-1}, slightly

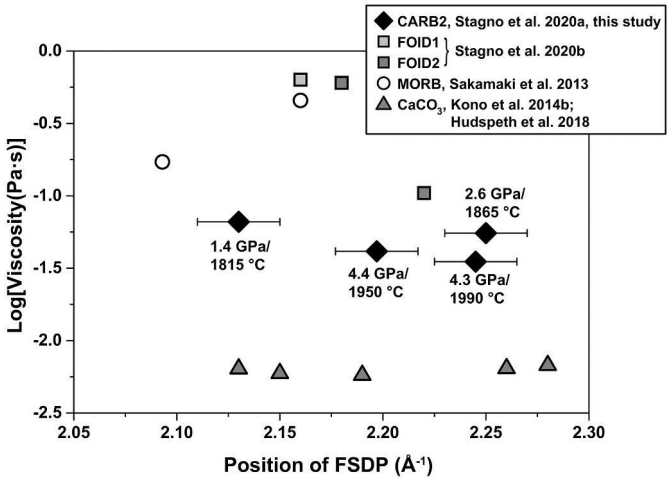

Fig. 8. Dependance of viscosity on the position of the first sharp diffraction peak (FSDP) in the structure factor for carbonate-silicate liquids (this study, Stagno et al., 2020a), molten calcite (Hudspeth et al., 2018; Kono et al., 2014b), melilititic liquids (Stagno et al., 2020b) and MOR basaltic liquids (Sakamaki et al., 2013).

shifting depending on particle size, and Stakheev et al. (1995) determined that CO adsorbed on Pt/KL zeolite resulted in the formation of Pt carbonyl peaks at 2008, 2031 and 2068 cm^{-1}. Therefore, the presence of absorptions at 2022, 2041, 2050, 2062, 2087 cm^{-1} in CARB2_2_2016 and CARB2_4 (some occurring as shoulders rather than distinct peaks in the latter) led us to assign those bands to metal carbonyl complexes were Fe, Pt or a PtFe alloy may act as the CO ligand, coexisting with free CO as testified by the peak at 2210 cm^{-1} (Fig. 6). Likewise, carbonyls (+free CO) might be recognized also in the small peaks of Raman spectra at 2060, 2077 and 2145 cm^{-1}, with free CO at 2100 cm^{-1} (Fig. S16).

The investigation of Ca-rich carbonate-silicate glasses synthesized under fully oxidized conditions by Raman spectroscopy (Moussallam et al., 2016) showed that the region of (Si-Al)-O stretching vibration is mostly dominated in order by Q_0>Q_1>Q_2>Si-O^0 along with an intense and sharp peak $\nu_1CO_3^{2-}$ at ~1080 cm^{-1} attributed to C-O stretching. This general spectral profile for silicate units is observed for glasses with 24 wt% SiO_2 and variable CO_2 contents, as well as for glasses with 31–32 wt % SiO_2 and no CO_2. The increase of CO_2 content is marked by the increase in intensity of Q_1 at 10 wt% CO_2, and Si-O^0 at 18 wt% CO_2. In contrast, an estimate of the abundance of Q_n species obtained through IR peaks relative areas indicates that Q_2 and Q_0 are the most abundant species in CARB2 quenched glasses, and that the vibrations of CO_3^{2-} for ν_1 contribution is much less active with respect to the data from Moussallam et al. (2016). In particular, glasses with ~19 and 23 wt% SiO_2 and estimated volatile content of 28 and 19 wt%, respectively, have a higher abundance of Q_2 than Q_0 and Q_1 with Si-O^0 being more pronounced at higher volatiles content. The glass with ~31 wt% SiO_2 and ~ 7 wt% volatiles is characterized by intensities that vary with Q_2>Q_0>Q_1>Si-O^0 with a tiny contribution of $\nu_1CO_3^{2-}$. On the other hand, we cannot exclude that the increasing intensity of Si-O^0 in the glass with high CO_2 content (CARB_2_2016) results from the shift of the $\nu_1CO_3^{2-}$ band to lower wavenumbers pointing out, therefore, differences of C in bonding within the structure. A mechanism of CO_3^{2-} speciation by the formation of metal-carbonate frameworks deriving from carbonate ions strongly interacting with metal cations was proposed for the case of carbonate glasses by Genge et al. (1995) and reported to cause a shift in wavenumber. This could also occur in our glasses. Alternatively, the low intensity of $\nu_1CO_3^{2-}$ despite the high CO_2 content, which is testified by the prominent features of CO_3^{2-} bending and stretching vibrations in μ-R-FTIR spectra, saturation of μ-T-FTIR spectra and low EMPA totals, can be explained as due to the peculiar glass composition and experimental conditions which may affect carbonate polarizability, and for which we failed to employ the quantification model proposed by Morizet et al. (2013).

High P μ-R-FTIR investigation showed that as the quenched glasses undergo compression, the asymmetry of CO_3^{2-} is observed to decrease as testified by the decrease in splitting observed in the carbonate doublet from μ-R-FTIR and μ-T-FTIR (visible in $3\nu_3$ and $4\nu_4$ overtones, Fig. S19c), implying a rearrangement of the structure where the carbonate environment gradually becomes more ordered and the silicate network more packed.

Finally, the spectroscopic evidence of molecular carbonate coexisting with carbon monoxide, water and carbonyl points out the possibility that these volatile species can be all dissolved in CO_2-rich magmas and be exsolved upon decompression. Such evidence would require the investigation of similar glasses quenched at lower T than those of this study or the possibility to investigate spectroscopically similar liquids at high P-T. Despite the oxidized nature of the investigated carbonate-silicate melt (i.e., among the candidate metasomatic liquids at mantle conditions), the fo_2 calculated at carbon saturation (Huizenga, 2005) at the experimental P-T conditions (Table 1) vary between −3.2 and − 4.6 as normalized to the fayalite-magnetite-quartz reference buffer (Ballhaus et al., 1991). These fo_2 values indicate the lowest bound at which the dominant CO_2 would coexist with CO and H_2O volatile species in equilibrium with graphite based on our spectroscopic observations. The low $Fe^{3+}/\sum$Fe measured in one of the glasses can be explained in light of the formation of reduced $M_x(CO)_n$ carbonyl groups (M = Fe, Pt). According to Rengan (2023) a possible redox equilibrium involving Fe can be as follows,

$$Fe_2O_3 + 13\ CO = 2\ \ Fe(CO)_5 + 3\ CO_2 \quad (2)$$

or,

$$\underset{\text{alloy}}{Fe} + 5\underset{\text{liq}}{CO} = \underset{\text{liq}}{Fe(CO)_5} \quad (3)$$

Both reactions require the presence of CO in the carbonate-silicate liquid, the solubility of which is strongly controlled by the fo_2. In particular, the CO/CO_2 ratio increases as the fo_2 decreases until C saturation according to the equilibrium,

$$C + CO_2 = 2\ \ CO \quad (4)$$

These conditions are likely to have been reached when the Earth's upper mantle was more reduced than today such as during the Archaean when carbonate-silicate magmas formed by redox melting of a graphite saturated peridotite rock source (Aulbach and Stagno, 2016; Stagno and Aulbach, 2021) at higher T regime. Our results highlight the potential role of carbonate-silicate melts in carrying reduced C-O-H volatiles, some of which may be responsible for mobilizing platinum group elements.

5. Conclusions

In this study we investigated the structure of synthetic carbonate-silicate (transitional) liquids by in situ multi-angle energy dispersive X-ray diffraction at pressures from 1.4 to 4.4 GPa and temperatures between 1815 °C and 1990 °C. EDXD data indicate that the intermediate range ordering decreases with increasing P and T. The structural characteristics observed at HP-T imply that viscosity of carbonate-silicate melts depends on the medium-range structural order. Then, an ambient pressure characterization of the glassy products quenched from the carbonate-silicate melt at HP-T conditions was performed by micro-Raman and reflectance- and transmittance-micro-FTIR spectroscopies. Glasses contain SiO_2 amounts varying from 18.75 to 30.91 wt% and calculated volatile contents ranging between 27.72 and 6.68 wt% with SiO_2/Al_2O_3 of 7.2–8.3 and MgO/CaO of 1.9–4.2. Raman spectra suggest that the silicate network in the quenched glasses is dominated by Q_0 and Q_2 species. A decrease in wavenumber of C-O ν_3 vibrations for CO_3^{2-} along with a significant splitting of the carbonate doublet is observed in reflectance FTIR spectra compared to what has been previously observed for the silicate and carbonate glasses, that we interpret as due to a highly distorted environment surrounding the carbonate anion. Neither evidence of CO_3^{2-} acting as a network former nor C dissolved as molecular CO_2 is observed in our quenched carbonate-silicate glasses. However, we found evidence of C occurring as both free molecular CO and CO bound to Fe, Pt or FePt alloy to form metal carbonyl complexes. In situ cold compression at room T of one of the quenched glasses by DAC combined with micro-reflectance-FTIR showed an increase of the relative intensity of peaks characterizing the silicate region, suggesting a more polymerized glass structure as pressure increases. Such P-driven polymerization does not occur at simultaneous high P-T conditions where the high T acts more dominantly to stretch out the tetrahedra. The reduction of the splitting of the carbonate doublet upon cold-compression suggests that T is required to cause a distorted carbonate environment.

Supplementary data to this article can be found online at https://doi.org/10.1016/j.chemgeo.2024.122152.

CRediT authorship contribution statement

V. Stopponi: Writing – review & editing, Writing – original draft, Visualization, Investigation, Formal analysis. **A. D'Arco:** Investigation.

Y. Kono: Resources, Investigation. **F. Piccirilli:** Investigation. **B.T. Poe:** Writing – review & editing. **S. Lupi:** Supervision, Resources. **M. Nazzari:** Investigation. **L. Pappalardo:** Investigation. **G. Marras:** Investigation. **M. Zacchigna:** Resources. **C.E. Manning:** Writing – review & editing, Funding acquisition. **C. Romano:** Writing – review & editing, Resources. **V. Stagno:** Writing – review & editing, Supervision, Investigation, Funding acquisition, Conceptualization.

Declaration of competing interest

The authors declare that they have no known competing financial interests or personal relationships that could have appeared to influence the work reported in this paper.

Data availability

Data are available at https://data.mendeley.com/datasets/xjb67vhgmr/2.

Acknowledgements

This research was funded by Sapienza University of Rome through Fondi di Ateneo 2021, and the Deep Carbon Observatory (DCO) to V. Stagno. Portions of this work were performed at HPCAT (Sector 16), Advanced Photon Source (APS), Argonne National Laboratory. HPCAT operations are supported by DOE-NNSA's Office of Experimental Sciences. The Advanced Photon Source is a US Department of Energy (DOE) Office of Science User Facility operated for the DOE Office of Science by Argonne National Laboratory under Contract No. DEAC0206CH11357. FTIR measurements were performed at Elettra Sincrotrone Trieste (proposal n. 20190568). Technical support at beamline ID18 of ESRF is also acknowledged as well as access to BGI instruments during G.M. visiting program.

The authors are grateful to constructive comments from Y. Morizet and D. Giordano, and the anonymous reviewers.

References

Aiuppa, A., Casetta, F., Coltorti, M., Stagno, V., Tamburello, G., 2021. Carbon concentration increases with depth of melting in Earth's upper mantle. Nat. Geosci. 14, 697–703.

Amalberti, J., Sarda, P., Le Losq, C., Sator, N., Hammouda, T., Chamorro-Pérez, E., Guillot, B., Le Floch, S., Neuville, D.R., 2021. Raman spectroscopy to determine CO_2 solubility in mafic silicate melts at high pressure: haplobasaltic, haploandesitic and approach of basaltic compositions. Chem. Geol. 582, 120413.

Armstrong, L.S., Hirschmann, M.M., Stanley, B.D., Falksen, E.G., Jacobsen, S.D., 2015. Speciation and solubility of reduced C-O-H-N volatiles in mafic melt: implications for volcanism, atmospheric evolution, and deep volatile cycles in the terrestrial planets. Geochim. Cosmochim. Acta 171, 283–302.

Aulbach, S., Stagno, V., 2016. Evidence for a reducing Archean ambient mantle and its effects on the carbon cycle. Geology 44 (9), 751–754.

Ballhaus, C., Berry, R.F., Green, D.H., 1991. High pressure experimental calibration of the olivine–orthopyroxene–spinel oxygen geobarometer: implications for the oxidation state of the upper mantle. Contrib. Mineral. Petrol. 107, 27–40. https://doi.org/10.1007/BF00311183.

Blank, J.G., Brooker, R.A., 1994. Experimental studies of carbon dioxide in silicate melts: solubility, speciation and stable isotope behavior. Rev. Mineral. 30, 157–186.

Blundy, J., Melekhova, E., Ziberna, L., Humphreys, M.C., Cerantola, V., Brooker, R.A., Ulmer, P., 2020. Effect of redox on Fe–Mg–Mn exchange between olivine and melt and an oxybarometer for basalts. Contrib. Mineral. Petrol. 175 (11), 103.

Brandt, R.K., Hughes, M.R., Bourget, L.P., Truszkowska, K., Greenler, R.G., 1993. The interpretation of CO adsorbed on Pt/SiO_2 of two different particle-size distributions. Surf. Sci. 286 (1–2), 15–25.

Brey, G.P., Green, D.H., 1976. Solubility of CO_2 in olivine melilitite at high pressures and role of CO_2 in the Earth's upper mantle. Contrib. Mineral. Petrol. 55, 217–230.

Brey, G.P., Ryabchikov, I.D., 1994. Carbon dioxide in strongly silica undersaturated melts and origin of kimberlite magmas. Neus. Jb. Miner. Mh. H10, 449–463.

Brey, G.P., Bulatov, V.K., Girnis, A.V., Lahaye, T., 2008. Experimental melting of carbonated peridotite at 6–10 GPa. J. Petrol. 49 (4), 797–821.

Brey, G.P., Bulatov, V.K., Girnis, A.V., 2011. Melting of K-rich carbonated peridotite at 6–10 GPa and the stability of K-phases in the upper mantle. Chem. Geol. 281, 333–342.

Brooker, R.A., Kjarsgaard, B.A., 2011. Silicate–carbonate liquid immiscibility and phase relations in the system SiO_2-Na_2O-Al_2O_3-CaO-CO_2 at 0.1–2.5 GPa with applications to carbonatite genesis. J. Petrol. 52 (7&8), 1281–1305.

Brooker, R.A., Holloway, J.R., Hervig, R.L., 1998. Reduction in piston cylinder experiments: detection of carbon infiltration into platinum capsules. Am. Mineral. 83, 985–994.

Brooker, R.A., Kohn, S.C., Holloway, J.R., McMillan, P.F., Carroll, M.R., 1999. Solubility, speciation and dissolution mechanisms for CO_2 in melts on the $NaAlO_2$-SiO_2 join. Geochim. Cosmochim. Acta 63, 3549–3565.

Brooker, R.A., Kohn, S.C., Holloway, J.R., McMillan, P.F., 2001a. Structural controls on the solubility of CO_2 in silicate melts part I: bulk solubility data. Chem. Geol. 174, 225–239.

Brooker, R.A., Kohn, S.C., Holloway, J.R., McMillan, P.F., 2001b. Structural controls on the solubility of CO_2 in silicate melts. Part II: IR characteristics of carbonate groups in silicate glasses. Chem. Geol. 174, 241–254.

Brooker, R.A., Sparks, R.S.J., Kavanagh, J.L., Field, M., 2011. The volatile content of hypabyssal kimberlite magmas: some constraints from experiments on natural rock compositions. Bull. Volcanol. 73, 959–981.

Dalton, J.A., Presnall, D.C., 1998. Carbonatitic melts along the solidus of model lherzolite in the system CaO-MgO-Al_2O_3-SiO_2-CO_2 from 3 to 7 GPa. Contrib. Mineral. Petrol. 131, 123–135.

Dalton, J.A., Wood, B.J., 1993. The compositions of primary carbonate melts and their evolution through wallrock reaction in the mantle. Earth Planet. Sci. Lett. 119, 511–525.

Dasgupta, R., Hirschmann, M.M., 2006. Melting in the Earth's deep upper mantle caused by carbon dioxide. Nature 440, 659–662.

Dasgupta, R., Hirschmann, M.M., 2007. Effect of variable carbonate concentration on the solidus of mantle peridotite. Am. Mineral. 93, 370–379.

Dasgupta, R., Mallik, A., Tsuno, K., Withers, A.C., Hirth, G., Hirschmann, M.M., 2013. Carbon-dioxide-rich silicate melt in the Earth's upper mantle. Nature 493, 211–216.

De Grouchy, C.J.L., Sanloup, C., Cochain, B., Drewitt, J.W.E., Kono, Y., Crépisson, C., 2017. Lutetium incorporation in magmas at depth: changes in melt local environment and the influence on partitioning behavior. Earth Planet. Sci. Lett. 464, 155–165.

Di Genova, D., Sicola, S., Romano, C., Vona, A., Fanara, S., Spina, L., 2017. Effect of iron and nanolites on Raman spectra of volcanic glasses: a reassessment of existing strategies to estimate the water content. Chem. Geol. 475, 76–86.

Eggler, D.H., 1978. The effect of CO_2 upon partial melting of peridotite in the system Na_2O-CaO-Al_2O_3-MgO-SiO_2-CO_2 to 35 kb, with an analysis of melting in a peridotite-H_2O-CO_2 system. Am. J. Sci. 278, 305–343.

Eggler, D.H., Mysen, B.O., Hering, T.C., Holloway, J.R., 1979. The solubility of carbon monoxide in silicate melts at high pressures and its effect on silicate phase relations. Earth Planet. Sci. Lett. 43, 321–330.

Elliott, S.R., 1991. Origin of the first sharp diffraction peak in the structure factor of covalent glasses. Phys. Rev. Lett. 6 (67), 711–714.

Elliott, S.R., 1995. Second sharp diffraction peak in the structure factor of binary covalent network glasses. Phys. Rev. B 13 (51), 8599–8601.

Foley, S.F., Yaxley, G.M., Rosenthal, A., Buhre, S., Kiseeva, E.S., Rapp, R.P., Jacob, D.E., 2009. The composition of near-solidus melts of peridotite in the presence of CO_2 and H_2O between 40 and 60 kbar. Lithos 1125, 274–283.

Genge, M.J., Jones, A.P., Price, G.D., 1995. An infrared and Raman study of carbonate glasses-implications for the structure of carbonatite magmas. Geochim. Cosmochim. Acta 59, 927–937.

Ghosh, S., Othani, E., Litasov, K.D., Terasaki, H., 2009. Solidus of carbonated peridotite from 10 to 20 GPa and origin of magnesiocarbonatite melt in the Earth's deep mantle. Chem. Geol. 262, 17–28.

Ghosh, D.B., Karki, B.B., 2017. Transport properties of carbonated silicate melt at high pressure. Sci. Adv. 3, e1701840.

Ghosh, S., Litasov, K., Ohtani, E., 2014. Phase relations and melting of carbonated peridotite between 10 and 20 GPa: a proxy for alkali- and CO_2-rich silicate melts in the deep mantle. Contrib. Mineral. Petrol. 167, 964.

Girnis, A.V., Bulatov, V.K., Brey, G.P., 2011. Formation of Primary Kimberlite Melts – Constraints from Experiments at 6-12 GPa and Variable CO_2/H_2O.

Green, D.H., 2015. Experimental petrology of peridotites, including effects of water and carbon on melting in the Earth's upper mantle. Phys. Chem. Miner. 42, 95–122.

Grewal, Damanveer S., Dasgupta, Rajdeep, Farnell, Alexandra, 2020. The speciation of carbon, nitrogen, and water in magma oceans and its effect on volatile partitioning between major reservoirs of the solar system rocky bodies. Geochim. Cosmochim. Acta 280, 281–301.

Grzechnik, A., Zimmermann, H.D., Hervig, R.L., King, P.L., Mcmillan, P.F., 1996. FTIR micro-reflectance measurements of the CO_3^{2-} ion content in basanite and leucitite glasses. Contrib. Mineral. Petrol. 125, 311–318.

Gudfinnsson, G.H., Presnall, D.C., 2005. Continuous gradations among primary kimberlitic, carbonatitic, melilitic, basaltic, picritic, and komatiitic melts in equilibrium with garnet lherzolite at 3-8 GPa. J. Petrol. 46, 1645–1659.

Guillot, B., Sator, N., 2011. Carbon dioxide in silicate melts: a molecular dynamics simulation study. Geochim. Cosmochim. Acta 75 (7), 1829–1857.

Hammouda, T., 2003. High-pressure melting of carbonated eclogite and experimental constraints on carbon recycling and storage in the mantle. Earth Planet. Sci. Lett. 214, 357–368.

Hammouda, T., Keshav, S., 2015. Melting in the mantle in the presence of carbon: review of experiments and discussion on the origin of carbonatites. Chem. Geol. 418, 171–188.

Hudspeth, J., Sanloup, C., Kono, Y., 2018. Properties of molten $CaCO_3$ at high pressure. Geochem. Perspect. Lett. 7, 17–21.

Hugues, F., Bassett, J.M., Taarit, Y.B., Choplin, A., Primet, M., Rojas, D., Smith, A.K., 1982. Surface organometallic chemistry: formation of $HFe_3(CO)_{11}^-$ from $Fe_3(CO)_{12}$ and $Fe(CO)_5$ on silica, alumina, magnesia, and zinc oxide. J. Am. Chem. Soc. 104 (25), 7020–7024.
Huizenga, J.M., 2005. COH, an Excel spreadsheet for composition calculations in the C-O-H fluid system. Comput. Geosci. 31 (6), 797–800.
Keshav, S., Gudfinnsson, G.H., 2010. Experimentally dictated stability of carbonated oceanic crust to moderately great depths in the Earth: results from the solidus determination in the system CaO-MgO-Al_2O_3-SiO_2-CO_2. J. Geophys. Res. 115, B05205.
Keshav, S., Gudfinnsson, G.H., 2014. Melting phase equilibria of model carbonated peridotite from 8 to 12 GPa in the system CaO-MgO-Al_2O_3-SiO_2-CO_2 and kimberlitic liquids in the Earth's upper mantle. Am. Mineral. 99, 1119–1126.
King, P.L., Holloway, J.R., 2002. CO_2 solubility and speciation in intermediate (andesitic) melts: the role of H_2O and composition. Geochim. Cosmochim. Acta 66, 1627–1640.
King, P.L., McMillan, P.F., Moore, G., 2004. Infrared spectroscopy of silicate glasses with application to natural systems. In: King, P.L., Ramsey, M.S., Swayze, G.A. (Eds.), Infrared Spectroscopy in Geochemistry, Exploration Geochemistry and Remote Sensing, 33. Mineralogical Association of Canada, Quebec City, QC, Canada, pp. 93–133. Short Course Series.
Kiseeva, E.S., Yaxley, G.M., Hermann, J., Litasov, K.D., Rosenthal, A., Kamenetsky, V.S., 2012. An experimental study of carbonated eclogite at 3.5–5.5 GPa - implications for silicate and carbonate metasomatism in the cratonic mantle. J. Petrol. 53 (4), 727–759.
Kiseeva, E.S., Litasov, K.D., Yaxley, G.M., Ohtani, E., Kamenetsky, V.S., 2013. Melting and phase relations of carbonated eclogite at 9-21 GPa and the petrogenesis of alkali-rich melts in the deep mantle. J. Petrol. 50, 1555–1583.
Kono, Y., Irifune, T., Higo, Y., Inoue, T., Barnhoorn, A., Suetsugu, D., Bina, C., Inoue, T., Wiens, D., Jellinek, M., 2010. P-V-T relation of MgO derived by simultaneous elastic wave velocity and in situ X-ray measurements: a new pressure scale for the mantle transition region. Phys. Earth Planet. Inter. 183, 196–211.
Kono, Y., Park, C., Kenney-Benson, C., Shen, G., Wang, Y., 2014a. Towards comprehensive studies of liquids at high pressures and high temperatures: combined structure, elastic wave velocity, and viscosity measurements in the Paris-Edinburgh cell. Phys. Earth Planet. Inter. 228, 269–280.
Kono, Y., Kenney-Benson, C., Hummer, D., Ohfuji, H., Park, C., Shen, G., Wang, Y., Kavner, A., Manning, C.E., 2014b. Ultralow viscosity of carbonate melts at high pressures. Nat. Commun. 5, 5091.
Konschak, A., Keppler, H., 2014. The speciation of carbon dioxide in silicate melts. Contrib. Mineral. Petrol. 167, 1–13.
Le Losq, C., Neuville, D.R., Moretti, R., Roux, J., 2012. Determination of water content in silicate glasses using Raman spectrometry: implications for the study of explosive volcanism. Am. Mineral. 97, 779–790.
Le Losq, C., Mysen, B.O., Cody, G.D., 2015. Water and magmas: insights about the water solution mechanisms in alkali silicate melts from infrared, Raman, and ^{29}Si solid-state NMR spectroscopies. Prog. Earth Planet. Sci. 2, 22.
Litasov, K.D., Ohtani, E., 2009a. Phase relations in the peridotite-carbonate-chloride system at 7.0- 16.5 GPa and the role of chlorides in the origin of kimberlite and diamond. Chem. Geol. 262, 29–41.
Litasov, K.D., Ohtani, E., 2009b. Solidus and phase relations of carbonated peridotite in the system CaO-Al_2O_3-MgO-SiO_2-Na_2O-CO_2 to the lower mantle depths. Phys. Earth Planet. Inter. 177, 46–58.
Litasov, K.D., Ohtani, E., 2010. The solidus of carbonated eclogite in the system CaO-Al_2O_3-MgO-SiO_2-Na_2O-CO_2 to 32 GPa and carbonatite liquid in the deep mantle. Earth Planet. Sci. Lett. 295, 115–126.
Long, D.A., 1977. Raman Spectroscopy. McGraw Hill.
Lupi, S., Nucara, A., Perucchi, A., Calvani, P., Ortolani, M., Quaroni, L., Kiskinova, M., 2007. Performance of SISSI, the infrared beamline of the ELETTRA storage ring. J. Opt. Soc. Am. B 24 (4), 959–964, 24959.
Mao, H.-K., Xu, J., Bell, P.M., 1986. Calibration of the ruby pressure gauge to 800 kbar under quasi-hydrostatic conditions. J. Geophys. Res. 91 (B5), 4673–4676.
Matson, D.W., Sharma, S.K., Philpotts, J.A., 1983. The structure of high-silica alkali-silicate glasses. A Raman spectroscopic investigation. J. Non-Cryst. Solids 56, 323–352.
McMillan, P.F., 1985. Vibrational spectroscopy in the mineral sciences. In: Kieffer, S.W., Navrotsky, A. (Eds.), Microscopic to Macroscopic: Atomic Environments to Mineral Thermodynamics. (Reviews in Mineralogy Vol 14). Mineralogical Society of America, Washington DC, pp. 9–63.
McMillan, P.F., Wolf, G., 1995. Vibrational spectroscopy of silicate liquids. In: Stebbins, J., McMillan, P., Dingwell, D. (Eds.), Structure, Dynamics and Properties of Silicate Melts, 32. Reviews in Mineralogy, Mineralogical Society of America, Chantilly, Virginia, pp. 247–315.
Mitchell, R.H., 1986. Kimberlites: Mineralogy, Geochemistry, and Petrology. Plenum, New York.
Mitchell, R.H., 1996. The melilitite clan. In: Mitchell, R.H. (Ed.), Undersaturated Alkaline Rocks: Mineralogy, Petrogenesis, and Economic Potential. Mineralogical Association of Canada, Short Course Series, 24, pp. 123–151.
Moore, G., Chizmeshya, A., McMillan, P.F., 2000. Calibration of a reflectance FTIR method for determination of dissolved CO_2 concentration in rhyolitic glasses. Geochim. Cosmochim. Acta 64 (20), 3571–3579.
Moore, K.R., Wood, B.J., 1998. The transition from carbonate to silicate melts in the CaO-MgO-SiO_2-CO_2 system. J. Petrol. 39, 1943–1951.
Morizet, Y., Brooker, R.A., Iacono-Marziano, G., Kjarsgaard, B.A., 2013. Quantification of dissolved CO_2 in silicate glasses using micro-Raman spectroscopy. Am. Mineral. 98, 1788–1802.
Morizet, Y., Paris, M., Sifré, D., Di Carlo, I., Gaillard, F., 2017a. The effect of Mg concentration in silicate glasses on CO_2 solubility and solution mechanism: implication for natural magmatic systems. Geochim. Cosmochim. Acta 198, 115–130.
Morizet, Y., Paris, M., Sifre, D., di Carlo, I., Ory, S., Gaillard, F., 2017b. Towards the reconciliation of viscosity change and CO_2-induced polymerization in silicate melts. Chem. Geol. 458, 38–47.
Moussallam, Y., Morizet, Y., Massuyeau, M., Laumonier, M., Gaillard, F., 2015. CO_2 solubility in kimberlite melts. Chem. Geol. 418, 198–205.
Moussallam, Y., Florian, P., Corradini, D., Morizet, Y., Sator, N., Vuilleumier, R., Guillot, B., Iacono-Marziano, G., Schmidt, B.C., Gaillard, F., 2016. The molecular structure of melts along the carbonatite–kimberlite–basalt compositional joint: CO_2 and polymerization. Earth Planet. Sci. Lett. 434, 129–140.
Mysen, B.O., Richet, P., 2019. Silicate Glasses and Melts, 2nd ed. Elsevier Science, p. 728.
Mysen, B.O., Arculus, R.J., Eggler, D.H., 1975. Solubility of carbon dioxide in melts of andesite, tholeiite, and olivine nephelininte composition to 30 kbar pressure. Contrib. Mineral. Petrol. 53, 227–239.
Mysen, B.O., Finger, L.W., Virgo, D., Seifert, F.A., 1982. Curve-fitting of Raman spectra of silicate glasses. Am. Mineral. 67, 686–695.
Ni, H.W., Keppler, H., 2013. Carbon in silicate melts. In: Hazen, R.M., Jones, A.P., Baross, J.A. (Eds.), Carbon in Earth Rev. Mineral Geochem, 75, pp. 251–287.
Ohashi, T., Sakamaki, T., Funakoshi, K.I., Suzuki, A., 2018. Pressure-induced structural changes of basaltic glass. J. Mineral. Petrol. Sci. 113, 286–292.
Partzsch, G.M., Lattard, D., McCammon, C., 2004. Mössbauer spectroscopic determination of Fe^{3+}/Fe^{2+} in synthetic basaltic glass: a test of empirical fO_2 equations under superliquidus and subliquidus conditions. Contrib. Mineral. Petrol. 147, 565–580.
Piccirilli, F., Mangialardo, S., Postorino, P., Baldassarre, L., Lupi, S., Perucchi, A., 2012. Sequential dissociation of insulin amyloids probed by high pressure Fourier transform infrared spectroscopy. Soft Matter 8 (11), 863.
Piriou, B., Arashi, H., 1980. Raman and infrared investigations of lead silicate glasses. High Temp. Sci. 13, 299–313.
Potapkin, V., Chumakov, A.I., Smirnov, G.V., Celse, J.P., Rüffer, R., McCammon, C., Dubrovinsky, L., 2012. The ^{57}Fe synchrotron Mössbauer source at the ESRF. J. Synchrotron Radiat. 19 (4), 559–569.
Prescher, C., McCammon, C., Dubrovinsky, L., 2012. MossA: a program for analyzing energy-domain Mössbauer spectra from conventional and synchrotron sources. J. Appl. Crystallogr. 45 (2), 329–331.
Price, S.E., Russell, J.K., Kopylova, M.G., 2000. Primitive magma from the Jericho pipe, N.W.T., Canada: constraints on primary kimberlite melt chemistry. J. Petrol. 41, 789–808.
Rengan, R., 2023. Metal carbonyls: synthesis, properties, and structure. In: Verma, D.K., Aslam, J. (Eds.), Organometallic Compounds.
Ritter, X., Guillot, B., Sator, N., Desmaele, E., Massuyeau, M., Sanchez-Valle, C., 2021. Non-Arrhenian temperature-dependent viscosity of alkali(ne) carbonate melts at mantle pressures. Front. Earth Sci. 9, 674770.
Rock, N.M.S., 1991. Lamprophyres. Blackie, Glasgow.
Rohrbach, A., Schmidt, M.W., 2011. Redox freezing and melting in the Earth's deep mantle resulting from carbon–iron redox coupling. Nature 472, 209–212.
Sakamaki, T., Suzuki, A., Terasaki, H., Urakawa, S., Katayama, Y., Funakoshi, K., et al., 2013. Ponded melt at the boundary between the lithosphere and asthenosphere. Nat. Geosci. 6, 1041–1044.
Shee, S.R., 1986. The Petrogenesis of the Wesselton Mica Kimberlites, Kimberley, South Africa. Ph.D. thesis. University of Cape Town.
Shishkina, T.A., Botcharnikov, R.E., Holtz, F., Almeev, R.R., Jazwa, A.M., Jakubiak, A.A., 2014. Compositional and pressure effects on the solubility of H_2O and CO_2 in mafic melts. Chem. Geol. 388, 112–129.
Socrates, G., 2004. Infrared and Raman Characteristic Group Frequencies: Tables and Charts, 3rd ed. Wiley, Chichester, England.
Stagno, V., Aulbach, S., 2021. Redox processes before, during and after Earth's accretion affecting the deep carbon cycle. In: Magma Redox Geochemistry. AGU Monograph, pp. 19–32.
Stagno, V., Frost, D.J., 2010. Carbon speciation in the asthenosphere: experimental measurements of the redox conditions at which carbonate-bearing melts coexist with graphite or diamond in peridotite assemblages. Earth Planet. Sci. Lett. 30, 72–84.
Stagno, V., Kono, Y., Stopponi, V., Masotta, M., Scarlato, P., Manning, C.E., 2020a. The viscosity of carbonate-silicate transitional melts at Earth's upper mantle P-T conditions by in-situ falling-sphere technique. In: Manning, C.E., Lin, J.-F., Mao, W. (Eds.), Carbon in Earth's Interior. AGU monographs.
Stagno, V., Stopponi, V., Kono, Y., D'Arco, A., Lupi, S., Romano, C., Poe, B.T., Foustoukos, D., Scarlato, P., Manning, Craig E., 2020b. The viscosity and atomic structure of volatile-bearing melilititic melts at high pressure and temperature and the transport of deep carbon. Minerals 10 (3), 267.
Stakheev, A.Y., Shpiro, E.S., Jaeger, N.I., Schulz-Ekloff, G., 1995. FTIR evidence of the formation of platinum carbonyls from Pt metal clusters encaged in KL zeolite. Catal. Lett. 34, 293–303.
Stanley, B.D., Hirschmann, M.M., Withers, A.C., 2014. Solubility of C-O-H volatiles in graphite-saturated Martian basalts. Geochim. Cosmochim. Acta 129, 54–76.
Tappe, S., Smart, K., Torsvik, T., Massuyeau, M., de Wit, M., 2017. Geodynamics of kimberlites on a cooling Earth: clues to plate tectonic evolution and deep volatile cycles. Earth Planet. Sci. Lett. 484, 1–14.
Trusheim, M.R., Jackson, R.L., 1983. Observation of photochemical intermediates in the low-temperature photolysis of silica-adsorbed iron carbonyl ($Fe(CO)_5$). J. Phys. Chem. 87 (11), 1910–1916.

Van Achterbergh, E., Griffin, W.L., Ryan, C.G., O'Reilly, S.Y., Pearson, N.J., Kivi, K., Doyle, B.J., 2002. Subduction signature for quenched carbonatites from the deep lithosphere. Geology 30, 743–746.
Van Achterbergh, E., Griffin, W.L., Ryan, C.G., O'Reilly, S.Y., Pearson, N.J., Kivi, K., Doyle, B.J., 2004. Melt inclusions from the deep Slave lithosphere: implications for the origin and evolution of mantle-derived carbonatite and kimberlite. Lithos 76, 461–474.
Vuilleumier, R., Seitsonen, A.P., Sator, N., Guillot, B., 2015. Carbon dioxide in silicate melts at upper mantle conditions: insights from atomistic simulations. Chem. Geol. 418, 77–88.
Wallace, M.E., Green, D.H., 1988. An experimental determination of primary carbonatite magma composition. Nature 335, 343–346.
Walter, M.J., 1998. Melting of garnet peridotite and the origin of komatiite and depleted lithosphere. J. Petrol. 39, 29–60.
Wang, Y., Sakamaki, T., Skinner, L.B., Jing, Z., Yu, T., Kono, Y., Park, C., Shen, G., Rivers, M.L., Sutton, S.R., 2014. Atomistic insight into viscosity and density of silicate melts under pressure. Nat. Commun. 5.
Weidendorfer, D., Manning, C.E., Schmidt, M.W., 2020. Carbonate melts in the hydrous upper mantle. Contrib. Mineral. Petrol. 175, 72. https://doi.org/10.1007/s00410-020-01708-x.
Wetzel, D.T., Rutherford, M.J., Jacobsen, S.D., Hauri, E.H., Saal, A.E., 2013. Degassing of reduced carbon from planetary basalts. Proc. Natl. Acad. Sci. 110, 8010–8013.
Wilding, M.C., Phillips, B.I., Wilson, M., Sharma, G., Navrotsky, A., Bingham, P.A., Brooker, R., Parise, J.B., 2019. The structure and thermochemistry of K_2CO_3-$MgCO_3$ glass. J. Mater. Res. 34 (19), 3377–3388.
Wyllie, P.J., Huang, W.-L., 1976. Carbonation and melting reactions in the system CaO-MgO-SiO_2-CO_2 at mantle pressures with geophysical and petrological applications. Contrib. Mineral. Petrol. 54, 79–107.
Xu, Q., 2002. Metal carbonyl cations: generation, characterization and catalytic application. Coord. Chem. Rev. 231 (1–2), 83–108.
Yaxley, G.M., Brey, G.P., 2004. Phase relations of carbonate-bearing eclogite assemblages from 2.5 to 5.5 GPa: implications for petrogenesis of carbonatites. Contrib. Mineral. Petrol. 146, 606–619.
Yoshioka, T., McCammon, C., Shcheka, S., Keppler, H., 2015. The speciation of carbon monoxide in silicate melts and glasses. Am. Mineral. 100, 1641–1644.
Yoshioka, T., Nakashima, D., Nakamura, T., Shcheka, S., Keppler, H., 2019. Carbon solubility in silicate melts in equilibrium with a CO-CO_2 gas phase and graphite. Geochim. Cosmochim. Acta 259, 129–143.
Zhou, M., Andrews, L., Bauschlicher, C.W., 2001. Spectroscopic and theoretical investigations of vibrational frequencies in binary unsaturated transition-metal carbonyl cations, neutral, and anions. Chem. Rev. 101, 1931–1962.